

國立臺灣大學工學院暨醫學院醫學工程學系

博士論文

Department of Biomedical Engineering

College of Engineering and College of Medicine

National Taiwan University

Doctoral Dissertation



應用脈衝式超音波熱治療與氯喹強化癌症奈米藥物治療

Enhancing Cancer Tumor Treatment of Nanomedicine with
Pulsed-wave Ultrasound Hyperthermia and Chloroquine

江季峰

Chi-Feng Chiang

指導教授：林文澧 博士

Advisor: Win-Li Lin, Ph.D.

中華民國 108 年 10 月

October 2019

國立臺灣大學博士學位論文
口試委員會審定書

應用脈衝式超音波熱治療與氯喹強化癌症奈米藥物治療

Enhancing Cancer Tumor Treatment of Nanomedicine with
Pulsed-wave Ultrasound Hyperthermia and Chloroquine

本論文係江季峰君（學號 F99548050）在國立臺灣大學醫學工程學系完成之博士學位論文，於民國 108 年 10 月 24 日承下列考試委員審查通過及口試及格，特此證明

口試委員：

林 乙 博

（指導教授）

王 季 峰

劉 希 楷

高 俊 良

黃 義 侑

張 富 雄

陳 景 欣

系主任：

致謝



感謝指導教授林文灃老師多年來的悉心指導，不只指引研究方向，更以身作則示範了不停探索新研究主題的做學問態度。

感謝聖凱學長、為中、芷君學姊，在研究和實驗方面提供了許多寶貴建議與技術指導。感謝梁博欽醫師伉儷在研究及生活方面提供的各種協助。也感謝實驗室學弟妹們在事務上的分擔幫忙，讓我在博士生涯最後幾年能專心致力於研究上。

感謝我的家人們，從我決定棄醫從研的時候開始，一直以來都無條件地支持我。

最後，也是最感謝的，是我親愛的妻子齡齡。沒有妳的陪伴、鞭策、與鼓勵，這篇論文肯定無法完成。



摘要

熱治療結合化療藥物為一有效之腫瘤治療策略，能強化奈米藥物穿透進入腫瘤組織並強化其療效。本研究分為兩部分，第一部分探討脈衝式超音波熱治療是否可增強 PEGylated liposomal doxorubicin (PLD) 對於轉移乳癌模式之療效。本實驗使用小鼠乳癌細胞 4T1 種植於 BALB/c 小鼠腦部，以活體影像系統追蹤腫瘤成長。腫瘤植入後六天，投予 PLD 並於腫瘤區域施打脈衝式超音波熱治療。實驗結果顯示脈衝式超音波熱治療可增加 PLD 於腫瘤區域之累積。此外，化療藥物 PLD 加上脈衝式超音波熱治療能有效抑制腫瘤之生長，而免疫染色及細胞凋亡測試亦佐證其效用。此研究證實應用脈衝式超音波熱治療能促進化療藥物有效進入腦腫瘤組織並達到治療之效果。

第二部分則結合脈衝式超音波熱治療與自噬抑制劑 chloroquine (CQ) 以進一步強化奈米藥物之療效並抑制腫瘤之復發。自噬作用在腫瘤細胞經常扮演重要的存活機制，因此抑制自噬作用是一可能之腫瘤輔助治療策略。本實驗使用小鼠乳癌細胞 4T1 種植於 BALB/c 小鼠皮下，於腫瘤植入後第五天投予 PLD 與 CQ，並於腫瘤局部施打脈衝式超音波熱治療，之後觀察腫瘤的生長變化並追蹤其復發。實驗結果證實 CQ 能更加強化脈衝式超音波與奈米藥物對腫瘤的抑制效果，並且能延緩腫瘤復發的時間。免疫染色與西方點墨法也證實了 CQ 對腫瘤細胞能有效抑制自噬作用。此研究證實結合脈衝式超音波熱治療與 CQ 能更加強化奈米藥物之抗腫瘤效果，並能長期抑制腫瘤復發。

關鍵詞：脈衝式超音波熱治療，奈米藥物，doxorubicin，氯喹，自噬抑制，癌症，腫瘤

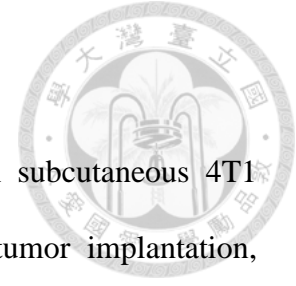


Abstract

Chemotherapeutic agents and hyperthermia are known to have synergistic effect in cancer treatment. Focused ultrasound sonication enhances the delivery of nanodrug into tumor and strengthens the efficacy of thermo-chemotherapy.

In the first part of our study, we investigated the enhancing effect of pulsed-wave ultrasound hyperthermia (pUH) on the delivery and therapeutic efficacy of PEGylated liposomal doxorubicin (PLD) for brain metastasis of breast cancer. Murine breast cancer cells 4T1 were implanted into mouse striatum as a metastatic brain tumor model, and the tumor growth was monitored with *in vivo* imaging system (IVIS). The mice were intravenously injected with PLD followed by transcranial pUH or continuous ultrasound hyperthermia (cUH) treatment on day-6 after tumor implantation. The amounts of doxorubicin accumulated in the normal brain and tumor tissues were measured with fluorometry. The tumor growth responses for the control, pUH, PLD, PLD+cUH, and PLD+pUH groups were evaluated with IVIS. The PLD distribution and cell apoptosis were assessed with immunofluorescence staining. The results showed that pUH significantly enhanced the PLD delivery into brain tumors and the tumor growth was further inhibited by PLD+pUH without damaging the sonicated normal brain tissues. This indicates that low-dose transcranial pUH is a promising method to selectively enhance nanodrug delivery and improve the brain tumor treatment.

In the second part of our study, we combined pUH and an autophagy inhibitor chloroquine (CQ) to further strengthen the antitumor efficacy of PLD and postponed the recurrence of tumor. Autophagy often serves as an important surviving mechanism for cancer cells, therefore inhibiting autophagy has been considered as an adjuvant



anti-cancer strategy. In this study, BALB/c mice implanted with subcutaneous 4T1 tumor were used as an animal tumor model. On Day 5 after tumor implantation, tumor-bearing mice received intravenous injection of PLD (10 mg/kg) plus 15-minute on-tumor pUH and were then fed with CQ (50 mg/kg daily) thereafter. It was shown that prolonged suppression of tumor growth was attained with PLD+pUH+CQ treatment, whereas in PLD+pUH group tumors quickly recurred after an initial inhibition. Immunohistochemical staining and Western blotting showed that autophagy of cancer cells was blocked for the mice receiving CQ. This study proves that PLD+pUH+CQ is a promising strategy to treat cancer for a sustained inhibition.

Keywords: pulsed-wave ultrasound hyperthermia, nanodrug, doxorubicin, chloroquine, autophagy inhibition, cancer, tumor

Contents

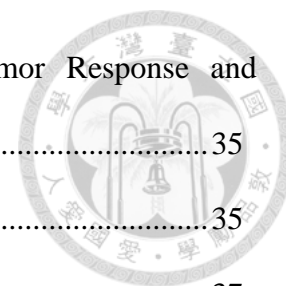


口試委員審定書	i
致謝	ii
中文摘要	iii
Abstract.....	iv
Contents.....	vi
List of Figures.....	x
List of Tables	xv
Chapter 1. Background & Objectives	1
1.1 Difficulties in cancer treatment	1
1.2 Cancer nanomedicine	2
1.2.1 Preferential accumulation due to EPR effect.....	2
1.2.2 Prolonged circulation time of PEGylated liposomes.....	3
1.2.3 Synergy between hyperthermia and of nanomedicine	4
1.3 Ultrasound Hyperthermia	4
1.3.1 Thermal effect of ultrasound	5
1.3.2 Ultrasound hyperthermia-enhanced drug delivery	6
1.3.3 Non-thermal effects of ultrasound.....	6
1.4 Autophagy inhibition in cancer treatment	7
1.5 Objectives	8
1.6 Thesis outline.....	8
Chapter 2. Pulsed-wave Ultrasound Hyperthermia Selectively Facilitates the Delivery of PEGylated Liposomal Doxorubicin and Improves the Antitumor Efficacy against Brain Metastasis of Breast Cancer	10

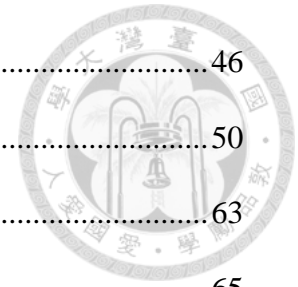
2.1 Introduction	10
2.2 Materials and Methods	12
2.2.1 PEGylated liposomal doxorubicin (PLD).....	12
2.2.2 <i>In vitro</i> investigation of PLD accumulation in cancer cells enhanced by ultrasound	13
2.2.3 Preparation of tumor cells and the brain tumor model	14
2.2.4 Focused ultrasound (FUS) system and pulsed-waved FUS hyperthermia	14
2.2.5 Experimental grouping	15
2.2.6 Quantification of PLD entering the normal brain and tumor tissues.....	15
2.2.7 Measurement of tumor growth by <i>in vivo</i> imaging system (IVIS) and mouse survival.....	16
2.2.8 Immunofluorescence and PLD distribution.....	16
2.2.9 TUNEL assay	17
2.2.10 Statistical analysis	17
2.3 Results	18
2.3.1 Pulsed-wave ultrasound better enhances PLD delivery into tumor cells	18
2.3.2 Low-dose pulsed-wave ultrasound hyperthermia enhances the antitumor action in brain tumors	18
2.3.3 PLD delivery to normal brain and tumor tissues by low-dose pulsed-wave/continuous-wave ultrasound hyperthermia.....	19
2.3.4 Immunofluorescence detection of PLD deposition	20
2.3.5 TUNEL staining for apoptotic cancer cells in the tumors	20
2.4 Discussion.....	21
2.5 Conclusions	24

Chapter 3. Pulsed-wave Ultrasound Hyperthermia Enhanced Nanodrug Delivery

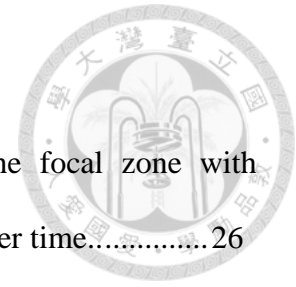
Combined with Chloroquine Exerts Effective Antitumor Response and Postpones Recurrence	35
3.1 Introduction	35
3.2 Materials and Methods	37
3.2.1 Chemical Reagents	37
3.2.2 Tumor cells	37
3.2.3 <i>In vitro</i> fluorescence assay of PLD internalization by 4T1 cells with or without CQ	37
3.2.4 MTT Cytotoxicity Assay	38
3.2.5 <i>In vivo</i> tumor model	39
3.2.6 Animal treatment experiment	39
3.2.7 Histopathological Examination and Immunohistochemical Study	40
3.2.8 TUNEL Assay	41
3.2.9 Western Blotting	42
3.2.10 Statistical analysis	42
3.3 Results	43
3.3.1 <i>In vitro</i> fluorescence assay of PLD internalization by 4T1 cells with or without CQ	43
3.3.2 MTT Cytotoxicity Assay	43
3.3.3 Combination treatment of PLD+pUH and CQ inhibited cancer tumor growth and delayed its recurrence	43
3.3.4 Immunohistochemical study proved autophagy of tumor cells blockaded by CQ administration	44
3.3.5 TUNEL assay showed apoptosis increased by PLD+pUH, not by CQ ..	45
3.3.6 Western Blotting	45



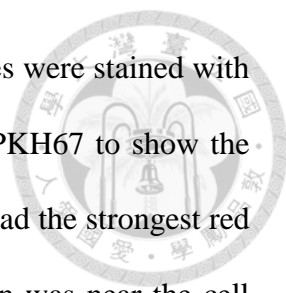
3.4 Discussion.....	46
3.5 Conclusions	50
Chapter 4. Summary and Future Work.....	63
References	65



List of Figures



- Figure 2-1. Typical temperature responses were measured at the focal zone with continuous wave or pulsed-wave ultrasound sonication over time.....26
- Figure 2-2. (A) Time course for the therapeutic experiments. 4T1 cancer cells were implanted on day 0, and the treatments were performed on day 6 with PLD injection, and/or continuous-wave ultrasound hyperthermia (cUH) or pulsed-wave ultrasound hyperthermia (pUH). IVIS imaging was performed on day 5, 7, 9, 11, 13 and 15. (B) Schedule for doxorubicin (Dox) quantification or immunofluorescence (IF) after different therapeutics.27
- Figure 2-3. Immunofluorescence staining for *in vitro* investigation of PEGylated liposomal doxorubicin (PLD) up-taken by 4T1 breast tumor cells with or without ultrasound sonication. Fluorescence staining of tumor cells was performed 2 h after different therapeutics: 1) control: no treatment; 2) PLD: PLD alone; 3) PLD + cU: PLD plus continuous-wave ultrasound sonication; 4) PLD + pU: PLD plus pulsed-wave ultrasound sonication. A dose of 3 $\mu\text{g/ml}$ PLD was used in this experiment and the sonication duration was 3 min for both continuous- and pulsed-wave ultrasound with the same acoustic power (0.4 W). Red, blue and green colors represent PLD, cell nuclei and cell membrane, respectively. Scale bar = 200 μm 28
- Figure 2-4. (A) Representative IVIS imaging and (B) bioluminescent signal quantification of mouse brain tumors from day 5 to day 15 after tumor implanted. Mice were implanted with luciferase-expressing 4T1-luc2 breast cancer cells in the brains. Bioluminescent signals were quantified using an IVIS imaging system. Treatment was executed on day 6 after tumors



sacrificed 24 h after the treatment and then the brain tissues were stained with DAPI to visualize the tumor cell nuclei (blue) and with PKH67 to show the cell membrane (green). Tumors treated with PLD + pUH had the strongest red fluorescence expression and the deposition of doxorubicin was near the cell nuclei. Scale bars: 50 μ m.33

Figure 2-8. TUNEL staining was used to detect apoptotic cells in tumor tissues. Mouse brains were implanted with 4T1-luc2 tumor cells and the treatments were performed 6 days after tumors implanted. A dose of 3.5 mg/kg PLD was i.v. administered for these experiments. The mice were then sacrificed 24 h after the treatments and then brain tumor slices were obtained for staining. Tumor slices were firstly stained with terminal TUNEL (green) and then with DAPI to visualize the tumor cell nuclei (blue). The strong apoptotic signal was observed in the PLD + pUH group. Scale bar: 100 μ m.34

Figure 3-1. The scheme of PEGylated Liposomal Doxorubicin (PLD) + pulsed-wave Ultrasound Hyperthermia (pUH) + chloroquine (CQ) in cancer treatment.. 51

Figure 3-2. Time schedule of treatment experiment. PEGylated Liposomal Doxorubicin (PLD) was given intravenously on Day 5 after tumor implantation. Pulsed-wave ultrasound hyperthermia (pUH) was administered 10~15 minutes after PLD administration. Then mice were orally fed chloroquine (CQ) dissolved in drink water daily till experiment end.....52

Figure 3-3. (A) Fluorescent microscopic images of 4T1 murine breast cancer cells in vitro treated with PLD+CQ+H or PLD+H. Doxorubicin (red) distribution with respect to nuclei (blue, stained with Hoechst 33342 dye) were shown. (B) Mean fluorescent intensity of doxorubicin with respect to nucleus region area. Abbreviation: H: hyperthermia. ns: not significant.53

Figure 3-4. MTT Cytotoxicity Assay. The cell viability was reduced by PLD with hyperthermia in a dose-dependent manner. The addition of CQ (10 μ M) further potentiated the cytotoxicity of PLD+H comparing to the counterpart without CQ. **: p<0.01, ***: p<0.001. Abbreviation: H=hyperthermia.....54

Figure 3-5. (A) Representative photographs of tumor for each group. Region encircled by dashed line indicated tumor. Scale bar=1cm. (B) The response of subcutaneous 4T1 murine breast cancer to different treatment: PLD+pUH+CQ, PLD+pUH, CQ, and control groups. * denotes p<0.05, and ** denotes p<0.01 between PLD+pUH+CQ and PLD+pUH, respectively. .55

Figure 3-6. The Kaplan-Meier survival plot for PLD+pUH+CQ, PLD+pUH, CQ, and control groups.57

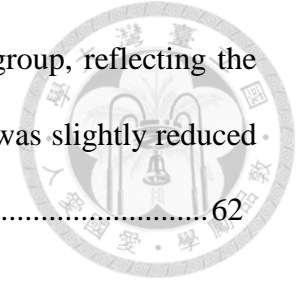
Figure 3-7. Histological examinations with hematoxylin-eosin staining for each experimental group. Scale bar = 100 μ m.58

Figure 3-8. Immunohistochemical stain for LC3 (brown stain) for each experimental group. LC3 accumulation reflects late-stage inhibition of autophagy. Greatly increased accumulation of LC3 was observed in both PLD+pUH+CQ and CQ groups, whereas slightly increase in the PLD+pUH group, and nearly no accumulation in the control group. Scale bar = 100 μ m.59

Figure 3-9. (A) Fluorescent microscopic images of TUNEL assay for each experimental group. Apoptotic signals (green) were much more enhanced in PLD+pUH+CQ group and PLD+pUH group. Scale bar = 200 μ m. (B) The fluorescent intensities for each experimental group were quantified and analyzed for statistical significance. **: p<0.01. ***: p<0.001. ns: not significant.....60

Figure 3-10. Western blot for LC3 for each experimental group. Increased expression of

LC3-II was observed in PLD+pUH+CQ group and CQ group, reflecting the late-stage autohphagy inhibition by CQ. LC3 expression was slightly reduced in PLD+pUH group comparing to control group.62



List of Tables

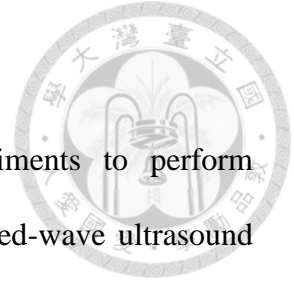


Table 2-1. Ultrasound parameters used in the <i>in vivo</i> experiments to perform continuous-wave ultrasound hyperthermia (cUH) or pulsed-wave ultrasound hyperthermia (pUH).	25
--	----

Chapter 1. Background & Objectives



1.1. Difficulties in cancer treatment

Cancer is a devastating threat to human health, causing the second leading number of death worldwide and responsible for an estimated 9.6 million deaths in 2018. Globally, about one in six deaths is due to cancer.

Several characteristics owned by cancer cells make them quite distinct from normal cells [1,2]. One of the most symbolic feature of cancer cells is its limitless replicative potential. Malignant cells proliferate dysregulated and form neoplasms that continue to grow. Besides, they also gain the ability to break basement membrane and invade adjacent tissue. Cancer cells can even travel via blood stream or lymphatic vessels for long distance to faraway sites where they may succeed in founding new colonies.

Recent studies indicate that cancer is not merely a collection of relatively homogenous malignant cells, but a complex structure which involves many types of cell, including endothelial cells, inflammatory cells, and stroma cells, etc. [2] This tumor microenvironment supports tumor growth and protects them from being attacked by host immune system. The sophisticated environment of cancer makes treating cancer a difficult challenge.

Furthermore, a small fraction of neoplastic cells, termed cancer stem cells (CSC), even aggravate the problem. Like normal tissue stem cells, CSCs may self-renew as well as spawn more differentiated descendent cells which forms the most part of bulk tumor. CSCs are capable of initiating a tumor even in very scarce numbers. Due to their relative quiescence in mitotic activity, CSCs have higher resistance to chemotherapy and radiotherapy, which often preferentially kill fast-dividing cells. Their persistence may be

responsible for the recurrence of cancer and make long-term cure of disease a challenging task.



1.2. Cancer nanomedicine

Chemotherapy remains the mainstream non-surgical treatment strategy against many types of cancer. Chemotherapeutic drugs target the signature characteristic of cancer cells by interrupting their division, hence malignant cells are no longer allowed to replicate limitlessly. However, the lack of specificity of conventional chemotherapeutic drugs limits their usefulness. A lot of chemotherapeutic drugs pose toxicity to normal organs, suppress immune system, and induce various adverse effects. These side effects not only impact on patients' life quality but also affect the feasible therapeutic dose, resulting in nonoptimal treatment.

The advance of nanotechnology provides a new opportunity to solve this problem [3,4,5]. By proper designing, nanoparticles can deliver chemotherapeutic drugs into cancer cells more efficiently and more specifically while minimizing the toxicity to normal cells. Nanomedicine can even simultaneously carry multiple functional moieties to facilitate chemotherapeutic drugs. Furthermore, nanomedicine possesses the potential to overcome drug resistance, since nanoparticles can bypass P-glycoprotein efflux pump, one of the main drug resistance mechanisms [5,6].

Nanoparticles used for cancer therapy can be made from a variety of materials, including polymers, liposomes, inorganic materials, etc. However, only a limited number of liposomes and polymer nanoformulations were clinically approved.

1.2.1. Preferential accumulation due to EPR effect

Owing to relatively large size, the delivery of nanomedicine is quite different from

that of molecular drug, which is mainly driven by diffusion. Nanomedicine preferentially accumulates in neoplastic tissues because of the enhanced permeability and retention (EPR) effect [2,7,8].

The EPR effect results from two key characteristics of the neoplastic tissues, the leaky vasculature and impaired lymphatic drainage [7,8]. Blood vessels in normal tissues are well-structured and lined by tight endothelial cells, which prevent nanoparticles from travelling through endothelium into tissue. However, in neoplastic tissue, the vasculature is structurally chaotic and defective in endothelial lining, thereby enabling nano-sized particles to pass through endothelial defects. Furthermore, the lack of functional lymphatic drainage allows nanoparticles to retain within tumor tissue for longer durations without being cleared. The EPR effect provides a way to preferentially deliver chemotherapeutic moieties into tumor while minimizing the adverse effects to normal tissue damage.

1.2.2. Prolonged circulation time of PEGylated liposomes

Despite the advantage of EPR effect, nanomedicine suffers from another problem. Nanoparticles entering circulation system are rapidly cleared by mononuclear phagocyte system (MPS) and quickly removed from blood stream, therefore they do not persist long enough to be delivered to target organ in sufficient dose [9].

To overcome such issue, long-circulating liposomes were invented. These liposomes carry long and flexible chains of hydrophilic polymers, e.g. poly-(ethylene glycol) (PEG), on their outer surface. The PEG chains occupy the peri-liposomal space and sterically exclude other macromolecules from getting close. Consequently, the binding of blood plasma opsonins to the liposome surface are hindered, and it renders these PEGylated liposomes ‘stealth’ to the surveillance of MPS [10]. The

pharmacokinetic half-life of stealth liposomes is hence greatly prolonged compared to conventional liposomes [11]. Stealth technology not only extends the circulation time of liposomes, but also changes their bio-distribution. PEGylated liposomes had a less uptake by liver and spleen while showed a higher plasma concentration as compared to conventional liposomes.

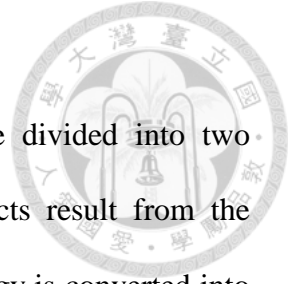
1.2.3. Synergy between hyperthermia and nanomedicine

Hyperthermia has been used in the treatment of many kinds of cancer for centuries [12,13]. Mildly elevating tissue temperature and maintaining it for several minutes can increase the blood flow and vascular permeability in the heated tumor region [14]. In addition, the uptake of chemotherapeutic drugs may be enhanced when cancer cells are placed at 43°C [15]. The delivery and uptake of nanomedicine at the target region can then be greatly enhanced using localized mild hyperthermia.

Furthermore, hyperthermia has been known to have synergistic effect with chemotherapeutic agents [15,16] or ionizing radiation [17]. Cancer cells can repair potentially lethal damage after exposure to chemotherapeutic drugs at 37°C, but at 43°C the repair ability was greatly hindered. Therefore, hyperthermia and chemotherapeutic nanomedicine can complement each other and form a good combination.

1.3. Ultrasound Hyperthermia

Ultrasound is a mechanical wave with frequencies higher than the audible range of human (20 kHz or greater). It oscillates and penetrates tissues, and is capable of carrying acoustic energy. Due to noninvasiveness and nonionizing radiation, ultrasound is widely used in medical applications, either as a diagnostic tool or therapeutic use.



1.3.1. Thermal effect of ultrasound

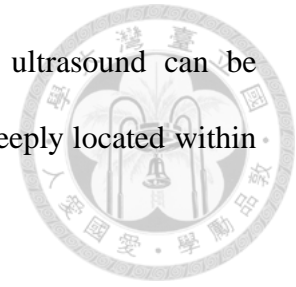
The effects of ultrasound dealt to biological tissues can be divided into two categories, thermal effects and non-thermal effects. Thermal effects result from the absorption of acoustic energy by tissues, and then the absorbed energy is converted into heat and it raises the temperature of tissues. A mild rise in temperature of biological tissues results in upregulated cellular metabolism and increase in blood flow, whereas a high rise in temperature can denature proteins and eventually cause coagulative necrosis. Different temperature rises lead to different clinical applications, e.g. mild temperature rises in adjuvant hyperthermia therapy, high temperature rises in ablation therapy, etc.

Cancer cells are more vulnerable to ultrasound exposure than normal cells [18]. Ultrasound can directly kill or sensitize cancer cells to stresses such as chemotherapeutic drugs or X-ray irradiation [19], and synergistic effects are observed when the temperature of cancer cells rises [20]. In addition, it has been reported that apoptosis was induced in several leukemia and lymphoma carcinoma cell lines *in vitro* by high-intensity pulsed ultrasound [21], low-intensity pulsed ultrasound [22], and ultrasound in combination with hyperthermia [23].

Along with the direct effects on tissues or cells, ultrasound hyperthermia can also activate host's immune system to fight against cancer. Hyperthermia induces anti-tumor immune response through complex mechanisms. It increases the expression of several potential tumor antigens, including MHC class I, heat shock proteins, and exosomes. Hyperthermia also stimulates immune cells, such as nature killer cells, CD8+ T cells, and dendritic cells. Along with these, the trafficking of immune cells between lymphoid organs and tumor are improved [12].

Ultrasound induced-hyperthermia was found to be more advantageous over other heating modalities due to its non-invasiveness and ability to penetrate into deep tissues

[24,25]. By tailoring transducer design, the acoustic energy of ultrasound can be precisely focused onto a very compact region even if the target is deeply located within body.



1.3.2. Ultrasound hyperthermia-enhanced drug delivery

During ultrasound sonication, the blood flow, elasticity and metabolic processes of the heated tumor are increased [26]. These effects facilitate the drug accumulation in the heated tumor region and improve the drug uptake by cancer cells through the release from thermal-sensitive forms [27] and/or through the membrane permeability modulation, especially for those cancer cells expressing multi-drug resistance [28]. The study of our group proved that short-time focused ultrasound hyperthermia (UH) could noninvasively enhance the permeability of BTB in the sonicated brain tumor region [29]. The results suggested that ultrasound sonication enhanced the delivery of PEGylated liposomal doxorubicin (PLD) into brain tumors and improved the treatment efficacy without damaging adjacent normal brain tissues.

1.3.3. Non-thermal effects of ultrasound

Non-thermal effects of ultrasound are usually associated with radiation force, acoustic streaming, and cavitation. Acoustic streaming and radiation pressure influence fluid and particle motion, causing convective microflow that can permeate cellular membrane and send particles into cells. Besides, ultrasound causes cavitation in the presence of gas-containing microbubbles. Cavitation is the oscillation of microbubbles in response to the pressure wave of ultrasound. Microbubbles repeatedly expand then contract, and may collapse violently when they grow beyond their critical sizes. The collapse, known as inertial cavitation, creates a brief but strong shockwave and causes

local a temperature rise. Additionally, free radicals are generated during cavitation by pyrolysis of molecules present inside collapsing microbubbles [30]. These phenomena can be utilized in several biomedical applications, such as blood-brain barrier disruption and sonodynamic therapy.

Pulsed-wave ultrasound was reported to further promote ultrasound-induced cancer cell apoptosis [31]. The pulse repetition frequency (PRF) might play a key role in ultrasound-induced biological and chemical effects [32]. Combination of doxorubicin and pulsed-wave ultrasound (PRF: 100 Hz) has been demonstrated its synergistic effects in cell killing and apoptosis enhancement in human lymphoma cells [16].

1.4. Autophagy inhibition in cancer treatment

Autophagy is a crucial catabolic process in maintaining homeostasis of cellular environment. It turns over old proteins and organelles and recycles cellular components [33,34]. Autophagy also plays an important role in cancer pathophysiology. The role of autophagy seems to be bi-directional depending on circumstances: it prevents cancer development, but helps established cancer to survive from stress and threats [33,34,35,36,37,38]. Therefore, autophagy inhibition has been investigated as an evolving strategy to fight against advanced cancer [37,38,39].

Among autophagy inhibitors, chloroquine (CQ) and its analogue hydroxychloroquine (HCQ) are the most widely used drugs. They inhibit lysosomal acidification and cause a late-stage blockade in autophagy [37]. In addition, CQ was reported to possess multiple anti-cancer mechanisms other than autophagy inhibition, such as targeting against cancer stem cells (CSC) [40] and inducing tumor vessel normalization [41]. There were several ongoing clinical trials using CQ (or HCQ) additional to conventional chemotherapeutic agents to treat various kinds of cancer,

including colorectal cancer, glioblastoma, and pancreatic cancer [38].



1.5. Objectives

The aim of present study is to develop an effective strategy capable of long-lastingly suppressing tumor growth and preventing cancer relapse. We implemented pulsed-wave ultrasound hyperthermia (pUH) to facilitate the delivery and activity of anti-cancer nanodrug against tumors. In addition, we utilized chloroquine to inhibit autophagy of cancer cells in order to prevent tumor recurrence.

The first part of study assesses the application of pUH to enhance the delivery and efficacy of anti-cancer nanodrug and evaluate treatment effectiveness in an intracranial brain metastatic tumor model.

The second part of study investigates the combination treatment of PLD with pUH and a constant CQ administration to successfully treat tumors, prevent tumor recurrence, and improve a disease-free survival.

1.6. Thesis outline

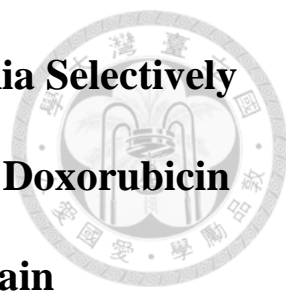
This dissertation is organized in four chapters. Chapter 1 provides an introduction of main topics to be addressed in this thesis. The application of cancer nanomedicine and enhanced delivery with ultrasound hyperthermia are briefly reviewed. Furthermore, the role of chloroquine, an autophagy inhibitor, in cancer treatment is introduced. Finally, the motivation and purpose of the thesis are described.

Chapter 2 focuses on the application of pulsed-wave ultrasound hyperthermia (pUH) to enhance the delivery and efficacy of PLD. The experiment setups in this study include *in vitro* fluorescent assay assessing PLD deposition, *in vivo* PLD quantification,

tumor growth evaluation with IVIS in an intracranial brain metastatic tumor model, and survival analysis.

Chapter 3 focuses on the addition of constant CQ administration along with PLD and pUH, to further improve the anti-tumor efficacy and prolong the disease-free survival. The experimental methods in this section include *in vitro* fluorescent assay investigating PLD internalization, MTT assay, Western blotting, immunohistochemistry study, and tumor growth in a subcutaneous tumor model.

Finally, Chapter 4 summarizes the research highlights of our studies and addresses the future work.



Chapter 2. Pulsed-wave Ultrasound Hyperthermia Selectively Facilitates the Delivery of PEGylated Liposomal Doxorubicin and Improves the Antitumor Efficacy against Brain Metastasis of Breast Cancer

2.1. Introduction

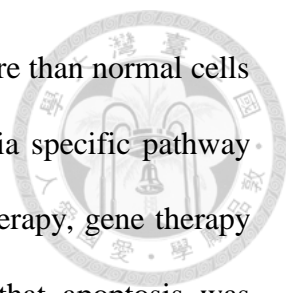
Elevating tissue temperature to a mild range and maintaining for several minutes can increase blood flow and drug absorption in the heated region [42]. Drug delivery and uptake at the target region can then be enhanced using localized mild hyperthermia. Ultrasound is a mechanical energy and it is a proved modality able to improve the tumor treatment outcome. Inhibition of many malignant tumors by hyperthermia alone [13] or in combination with other modalities was reported decades ago. Synergistic response was well-known when it came with ionizing radiation [17] and in combination with some chemotherapeutic agents [15]. Ultrasound induced-hyperthermia was also investigated [24] and found to be more beneficial than other heating modalities due to its facility in controlling focal power and tissue attenuation coefficient for deep tumor targeting [25].

Despite the fact that the blood-tumor barrier (BTB) is more permeable than the blood-brain barrier (BBB), the efficacy of systemic chemotherapy for the treatment of brain tumor is still hindered by BTB from achieving the therapeutic levels. It is also worth mention that the selectivity and heterogeneity of the BTB permeability blocks many chemotherapeutic agents from effectively accumulating in the target [43]. Therefore, it is necessary to develop powerful approaches to improve the delivery of

therapeutic agents to the target region with minimizing the side effects of critical tissues.

Short-time focused ultrasound hyperthermia (UH) could noninvasively enhance the permeability of BTB in the sonicated brain tumor region [29]. The results suggested that ultrasound sonication represented a feasible approach for enhancing PLD delivery into brain tumors and improved the treatment efficacy without damaging the normal brain tissues. It also reported that pulsed-wave ultrasound could promote ultrasound-induced cancer cell apoptosis [31]. The pulse repetition frequency (PRF) might play a key role in ultrasound-induced biological and chemical effects [32]. Combination of doxorubicin and pulsed-wave ultrasound (PRF: 100 Hz) has been demonstrated its synergistic effects in cell killing and apoptosis enhancement in human lymphoma cells [16].

Ultrasound can be a non-invasive, highly precise and deeply penetrating mechanical wave and has the potential to destroy tumor cells. For cancer therapy, ultrasound can directly kill or sensitize cancer cells to upcoming stresses, such as anticancer drugs or X-irradiation [19], and the synergistic effect also occurs when cancer cells suffer temperature rise [20]. This indicates that thermal effect is one of the key factors for ultrasound cancer treatment. During ultrasound sonication, the blood flow, elasticity and metabolic processes of the heated tumor are increased [26]. These would enhance the accumulation of drug in the heated tumor and the drug uptake for cancer cells through the release from thermal-sensitive forms [27] and/or through the membrane permeability modulation, especially for those cancer cells displaying multidrug resistance [28]. Therapeutic ultrasound was developed to deliver drugs and genes to a variety of tissues [44,45,46] and locations, such as tumors [47,48], cardiac tissues [49,50], and brain [51]. The alternate compressions and rarefactions of ultrasound produce a slight oscillation of fluid and tissues, which might increase cell membrane permeability [52] and molecular transport by altering molecular motion [53].



Cancer cells were more prone to be killed by ultrasound exposure than normal cells [18]. For cancer therapy, low-intensity ultrasound has been used via specific pathway interactions, such as sonoporation therapy [54], enhancing chemotherapy, gene therapy [16], and apoptotic therapy [55]. It has been recently reported that apoptosis was induced in several leukemia and lymphoma carcinoma cell lines *in vitro* by high-intensity pulsed ultrasound [21], low-intensity pulsed ultrasound [22], and ultrasound in conjunction with hyperthermia [23].

The aim of the present study was to develop pulsed-wave low-dose ultrasound hyperthermia and evaluate its treatment effectiveness for brain tumors. To determine whether pulsed-wave ultrasound was effective to deliver PLD into the sonicated tumor cells, we arranged an *in vitro* test for tumor cells exposed to ultrasound sonication under a constant temperature condition. Then, we arranged a focused ultrasound transducer to produce pulsed-wave/continuous-wave low-dose ultrasound hyperthermia in the target brain tumor after an I.V. PLD injection. We followed up the tumor growth response and measured the PLD depositions in brain and tumor tissues one day after the PLD injection with/without ultrasound hyperthermia.

2.2. Materials and Methods

2.2.1. PEGylated liposomal doxorubicin (PLD)

The PLD used in this study was a commercialized product, Lipo-Dox® purchased from Taiwan Tung Yang Biopharm Company Ltd. It contains 2 mg/mL doxorubicin and 14 mol/mL phospholipids. Its lipid composition is DSPC, cholesterol, and PEG-DSPE (molar ratio 3:2:0.3). The average particle size of the PLD is about 100 nm and its elimination half-life is 65 h.

2.2.2. *In vitro* investigation of PLD accumulation in cancer cells enhanced by ultrasound

Murine 4T1-luc2 breast cancer cells (ATCC® CRL-2539TM) expressing firefly luciferase (luc2 vector) were cultured in Dulbecco's Modified Eagle's Medium (DMEM) supplemented with 10% heat-inactivated fetal bovine serum (FBS), and penicillin (100 U/mL)/streptomycin (100 µg/mL) in 10 cm tissue culture plates in a 5% CO₂-containing incubator at 37 °C. Bioluminescence activity was confirmed using fluorometer. Cell number and viability were calculated using a hemocytometer and trypan blue exclusion.

To investigate PLD uptake by tumor cells, 10⁶ 4T1-luc2 cells with 1 mL PBS were loaded in an Eppendorf tube and prepared to receive ultrasound sonication. A dose of 3 µg/mL PLD was added to the Eppendorf tube before sonication. Ultrasound sonication was generated by a 500-kHz, single-element focused transducer (H104MR; Sonic Concepts, Bothell, WA, USA) with a diameter of 64 mm and a curvature radius of 62 mm. The radiofrequency signal was supplied by a function generator (33120A; Agilent, Palo Alto, CA, USA), and then the signal was amplified by a radiofrequency power amplifier (75A250A; Amplifier Research, Souderton, PA, USA). The acoustic wave was transmitted to the Eppendorf tube directly by a removable cone filled with degassed water. This experiment was composed of four groups: control (without PLD), PLD alone, PLD + cU (continuous-wave ultrasound), and PLD + pU (pulsed-wave ultrasound). For the PLD + pU group, a pulse repetition frequency (PRF) of 1000 Hz and a duty cycle of 50% were used. The sonication duration was 3 min and the acoustic power was 0.4 W for both the PLD + cU and PLD + pU groups. After sonication, tumor cells were incubated in a 12-well plate for 2 h in an incubator. An inverted fluorescence microscopy (Axiovert 200 M; Carl Zeiss Ltd., Oberkochen, Germany) was used to observe the PLD distribution in tumor cells after ultrasound sonication.

2.2.3. Preparation of tumor cells and the brain tumor model

All the experimental protocols were approved by the Institution of Animal Care and Use Committee, College of Medicine, National Taiwan University. Eight-week-old female BALB/c mice were housed with a 12-h light/dark cycle and allowed free access to water and standard diet. The mice were anesthetized by 1–3% isoflurane during the tumor implantation surgery. A total of 2×10^4 of 4T1-luc2 tumor cells suspended in 2 μ L of phosphate buffered saline (PBS) were slowly injected at a rate of 2 μ L/min into the right caudate putamen (0.5 mm anterior and 2.0 mm lateral to the bregma at a depth of 3 mm from the dura) over a 1-min duration. The needle was stayed for 5 min and then withdrawn for 1 min. The incision was sewn up with 6-0 polydioxanone suture.

2.2.4. Focused ultrasound (FUS) system and pulsed-waved FUS hyperthermia

Ultrasound was generated by a 500-kHz single-element focused transducer whose half-maximum pressure amplitude diameter and length of the focal zone were 3 mm and 8 mm, respectively. The radiofrequency signal was supplied by a function generator and then the signal was amplified by a radiofrequency power amplifier. The FUS was precisely targeted using a stereotaxic apparatus (Stoelting, Wood Dale, IL, USA). The center of the focal spot was approximately 3 mm below the cone tip. In the experiments, we used two types of ultrasound parameters to achieve ultrasound hyperthermia. Table 2-1 shows the detail of the parameters used for continuous-wave ultrasound hyperthermia (cUH) and pulsed-wave ultrasound hyperthermia (pUH). Fig. 2-1 shows the temperature responses at the focal zone measured with T-type thermocouple during cUH and pUH. The cumulated thermal doses (CEM43°C) for both cUH and pUH are less than 2 min.

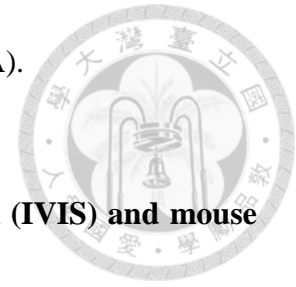
2.2.5. Experimental grouping

The *in vivo* experiments included two parts: part 1, tumor growth responses to various therapeutics (Fig. 2-2A); and part 2, quantification or immunofluorescence of PLD in normal brain and tumor tissues (Fig. 2-2B). Totally 55 mice were used for the PLD quantification and treatment studies. To examine the treatment efficacy, we used 25 mice randomly divided into five groups: 1) control (n = 5), 2) PLD alone (n = 5), 3) pUH alone (n = 5), 4) PLD + cUH (n = 5), and 5) PLD + pUH (n = 5). To quantify the amount of PLD deposited in the normal brain and tumor tissues, we used 30 mice randomly divided into six groups: 1) normal brain without hyperthermia (n = 5), 2) normal brain with cUH (n = 5), 3) normal brain with pUH (n = 5), 4) brain tumor without hyperthermia (n = 5), 5) brain tumor with cUH (n = 5), and 6) brain tumor with pUH (n = 5). The PLD was injected as a bolus (5 mg/kg) approximately 1 min before ultrasound hyperthermia.

2.2.6. Quantification of PLD entering the normal brain and tumor tissues

To investigate whether doxorubicin delivery was enhanced by continuous-wave or pulsed-wave ultrasound hyperthermia, a dose of 5 mg/kg PLD was administered through the tail vein on day 6 after tumor implantation with or without hyperthermia. To flush the PLD in the cerebral vessels, the brain was perfused with normal saline via a transcardial method 24 h after the PLD administration. The amounts of doxorubicin deposited in tissues were then quantified as our previous study [29]. To correct for background fluorescence, the samples were compared with standard curve data from the fluorescence emission of known amounts of doxorubicin added to acidified isopropanol extracts of homogenized tumor tissue from untreated mice. The concentration of doxorubicin was measured using a fluorometer (excitation at 470 nm and emission at

590 nm) (SpectraMax M2; Molecular Devices, Sunnyvale, CA, USA).



2.2.7. Measurement of tumor growth by *in vivo* imaging system (IVIS) and mouse survival

The mice were anesthetized with isoflurane and then D-luciferin (Gold Biotechnology Inc., St Louis, MO, USA) was intraperitoneally injected (150 mg/kg) at 10 min before imaging. The mice were imaged with an IVIS® Spectrum, and bioluminescent signals were quantified using Living Image 3.0 (Caliper Life Sciences, Alameda, CA, USA). Images were taken every other day starting from day 5 and continuing up to day 15 after tumor implantation. The treatment was performed on day 6 after tumor implantation when the measured bioluminescent value reached approximately 10^6 photons/s. The survival time of tumor-bearing mice was also evaluated. The survival data were analyzed by using log-rank test in the Kaplan-Meier analysis method and summarized by a means of median survival times with their 95% confidence intervals.

2.2.8. Immunofluorescence and PLD distribution

Immunofluorescence staining was accomplished on day 7 post-implantation. The mice were sacrificed, perfused with saline and then phosphate buffer containing 4% paraformaldehyde to fix the brain tissues. The brains were immersed with 4% paraformaldehyde at 4 °C overnight, and then moved to 30% sucrose solution at 4 °C for 2 days. The brains were sequentially sliced to a thickness of 20 μ m. Three representative slices for the maximal tumor area were taken for each group. For immunofluorescence analysis, tissue slices were pretreated with 4% formaldehyde and permeabilized with 20 μ g/mL proteinase K and 0.2% Triton X-100 in PBS. The slides

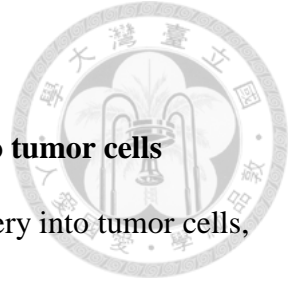
were then mounted with a solution containing blue 4',6-diamidino-2-phenylindole (DAPI) (Sigma, St Louis, MO, USA) and labeled with the PKH67 Green Fluorescent Cell Linker Kit (Sigma, St. Louis, MO). Doxorubicin fluorescent detection was carried out with a green excitation/red emission filter using a confocal microscope (Axio Imager A1; Carl Zeiss Ltd., Oberkochen, Germany). All images were captured using the same exposure time. The pictures were merged using AxioVision Rel. 4.8 software (Carl Zeiss Ltd., Oberkochen, Germany).

2.2.9. TUNEL assay

Tumor sections were processed for the terminal deoxynucleotidyl transferase dUTP nick end labeling (TUNEL) assay using a DeadEnd Fluorometric TUNEL system (Promega, Madison, WI, USA) following the manufacturer's instructions. Briefly, the slides were fixed with 4% formaldehyde and permeabilized with 20 µg/mL proteinase K and 0.2% Triton X-100 in PBS. The slides were then labeled with a TdT reaction mixture for 60 min in a 37 °C incubator and mounted with a mounting solution containing DAPI. Fluorescence images of apoptotic cells (green) and cell nuclei (blue) were obtained using a confocal microscope with the fluorescein isothiocyanate-DAPI setting. All images were captured using the same exposure time. The pictures were also merged using AxioVision Rel. 4.8 software.

2.2.10. Statistical analysis

All values are displayed as mean ± SEM (standard error of the mean). The results were analyzed with one-way analysis of variance with the post hoc Dunnett test. Statistical significance was defined as $p < 0.05$. Calculations were processed on a personal computer using SPSS version 20.0 (SPSS Inc., Chicago, Illinois, USA).



2.3. Results

2.3.1. Pulsed-wave ultrasound better enhanced PLD delivery into tumor cells

To investigate the effect of ultrasound sonication on PLD delivery into tumor cells, we utilized fluorescence microscopy to detect the PLD distribution. Fig. 2-3 showed that PLD delivery was enhanced by both pulsed-wave and continuous-wave ultrasound, and it displayed that pulsed-wave ultrasound could produce a much higher PLD deposition in tumor cells than continuous-wave ultrasound.

2.3.2. Low-dose pulsed-wave ultrasound hyperthermia enhanced the antitumor action in brain tumors

To investigate the effect of low-dose focused ultrasound hyperthermia (UH) on the anti-cancer action of PLD for brain tumor-bearing mice, a single treatment was executed on day 6 after tumor implantation. Tumor progression was then evaluated by an *in vivo* imaging system (IVIS) every other day starting from day 5. A dose of 3.5 mg/kg PLD was injected through tail vein before ultrasound hyperthermia. Fig. 2-4A showed the representative images of the bioluminescent signals, indicating that the photons increased exponentially in the control group. The PLD group and the pulsed-wave UH (pUH) alone group had a similar tumor growth pattern. In addition, the signal pattern for the PLD + cUH group (PLD plus continuous-wave UH (cUH)) showed a better inhibition of tumor growth than the PLD and pUH groups. As compared with the PLD + pUH group, the tumor inhibition was markedly better for PLD + pUH than PLD + cUH. Fig. 2-4B showed the results of the temporal bioluminescent response, indicating that the tumors treated with PLD + pUH were significantly inhibited on day 13 as compared with the PLD + cUH group. On day 15, the brain tumors in the other treatment groups grew out of the skull except for the PLD + pUH group. Tumors growing outside the

skull would lead to overestimated photon intensities, and hence there was only the PLD + pUH group shown on day 15.

Fig. 2-5 showed the survival response of the brain tumor-bearing mice treated with different therapeutics. The treatment with PLD + pUH led to a significantly improved survival time for the tumor-bearing mice, as compared with the control, PLD, pUH, and PLD + cUH groups. The median survival times for the mice treated with PLD, pUH, PLD + cUH or PLD + pUH were 16, 16, 17, 22 days, respectively, much longer than the control group (11 days). The prolonged survival time for the pUH group (same survival time as the PLD group) indicated that low-dose pulsed-wave focused ultrasound hyperthermia could damage brain tumors and result in a longer survival time than the control group. The prolonged survival time of the PLD + pUH group indicated that low-dose pulsed-wave ultrasound hyperthermia could both damage brain tumors and effectively enhance PLD delivery into the sonicated tumor cells/tissues to achieve the best anti-tumor activity.

2.3.3. PLD delivery to normal brain and tumor tissues by low-dose pulsed-wave/continuous-wave ultrasound hyperthermia

Fluorometry was used to measure the doxorubicin from the PLD deposited in the normal brain and tumor tissues for the mice with/without low-dose continuous-wave/pulsed-wave ultrasound hyperthermia. Fig. 2-6 showed the concentration of doxorubicin in the normal brain and tumor tissues 24 h after an injection of 5 mg/kg PLD. The doxorubicin concentration was significantly greater in the tumors treated with PLD + pUH than those in the tumors treated with PLD + cUH or PLD alone. This suggested that low-dose pulsed-wave ultrasound hyperthermia had the ability to significantly increase the PLD transport into the sonicated tumor tissues. This

figure also showed that there was no obvious difference of the PLD concentration in normal brain tissues among these three groups.



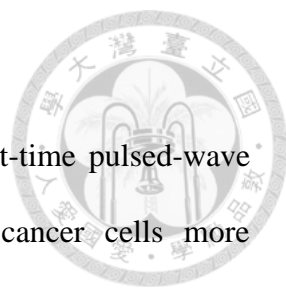
2.3.4. Immunofluorescence detection of PLD deposition

Fluorescence microscopy was used to study the deposition of the fluorescent PLD in tumor tissues for the PLD, PLD + cUH, and PLD + pUH groups 24 h after PLD injection. Labeling marker PKH67 (green color) was used to identify the cell membrane. Fig. 2-7, the results of immunofluorescence staining for tumor tissues, showed that the tumor sections for the PLD + pUH group had a more enriched doxorubicin (red color) accumulation than those for the PLD and PLD + cUH groups. The doxorubicin depositions were consistent with the quantification results of brain tumor tissues (Fig. 2-6).

2.3.5. TUNEL staining for apoptotic cancer cells in the tumors

To further assess the antitumor effect, TUNEL staining was performed to detect apoptotic cells in the tumors. Fig. 2-8 showed that the PLD + pUH group had the strongest TUNEL-positive signal among the PLD, PLD + cUH, and PLD + pUH groups, indicating that there were much more apoptotic cancer cells by applying a low-dose pulsed-wave ultrasound hyperthermia after PLD injection.

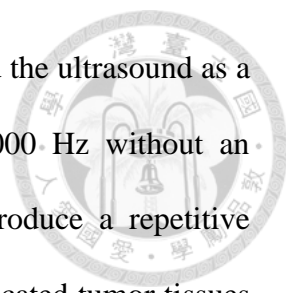
2.4. Discussion



In this study, we demonstrated in the *in vitro* study that short-time pulsed-wave ultrasound (pU) could enhance the PLD delivery into breast cancer cells more effectively than continuous-wave ultrasound (cU) under the same acoustic power and sonication duration (Fig. 2-3). In addition, we also showed in the *in vivo* study that low-dose pulsed-wave ultrasound hyperthermia (pUH) could result in a higher deposition of PLD in brain tumors than continuous-wave ultrasound hyperthermia (cUH) under the same acoustic power and sonication duration (Fig. 2-6 and Fig. 2-7). The combined effects of pulsed-wave ultrasound and ultrasound hyperthermia significantly improve the PLD delivery into the sonicated tumor tissues and cancer cells to produce a boosted cytotoxicity to inhibit the tumor growth (Fig. 2-4B and Fig. 2-8) and produce a higher survival for brain tumor-bearing mice (Fig. 2-5).

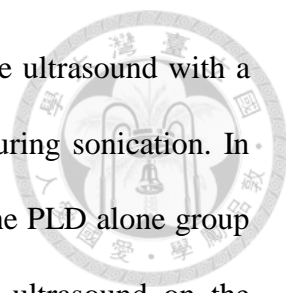
In a fluid or soft tissues, ultrasound propagates as a longitudinal wave of alternate compressions and rarefactions and it may cause direct mechanical effects on the sonicated tissues and cells. The alternate compressions and rarefactions of ultrasound may produce a slight oscillation of fluid and tissues, which might increase cell membrane permeability [32] and molecular transport by altering molecular motion [42]. In addition, a phenomenon called acoustic streaming occurs when the momentum of the sound waves transfers to an absorbing fluid, thus generating convective flow in the direction of the propagating ultrasonic waves. These phenomena may enhance cell membrane permeability and the transport of nanodrug into the sonicated cells to produce a higher concentration of PLD in the cancer cells as shown in Fig. 2-3 (the difference between the PLD group and the PLD + cU group).

There are several mechanisms whereby ultrasound sonication may be involved in drug delivery with/without the presence of microbubbles. In this study, we employed



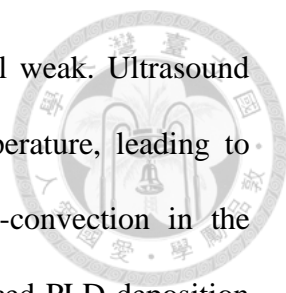
focused ultrasound to produce localized hyperthermia and modulated the ultrasound as a pulsed-wave form with a pulse repetition frequency (PRF) of 1000 Hz without an injection of microbubbles. This pulsed-wave ultrasound would produce a repetitive radiation pressure with a gradient around several Pa/mm on the sonicated tumor tissues and cancer cells. As a result, this repetitive radiation pressure would make the sonicated tumor tissues and cancer cells moving forwards and backwards. This may be the main reason for the *in vitro* experimental results showing that pulsed-wave ultrasound (pU) can produce a better cell membrane permeability and transport of nanodrug into the cancer cells to have a higher concentration of PLD in the sonicated cancer cells as shown in Fig. 2-3 (the difference between the PLD + cU group and the PLD + pU group). Similarly, pulsed-wave ultrasound hyperthermia improves the transport of PLD into the sonicated tumor tissues and gives an impact on the cancer cell membranes to have a better delivery of PLD into cancer tumors as shown in Fig. 2-4. Here, we demonstrated that the combined effects of pulsed-wave ultrasound and low-dose ultrasound hyperthermia could significantly improve the nanodrug delivery into the sonicated tumor and cancer cells to boost the cytotoxicity and the inhibition of tumor growth as shown in Fig. 2-4, Fig. 2-6 (the difference between the PLD + cUH group and the PLD + pUH group). Further study is necessary to optimize the ultrasound parameters, such as PRF, duty cycle, etc. and to visually examine the impact of pU on cell membrane functions.

The mechanical effects of alternate compressions and rarefactions of ultrasound sonication on the cell membrane may cause membrane deformation, poration, or sometimes lysis even in the absence of transient cavitation [32,56]. It reported that tumor suppressor protein, p53, might affect the integrality of the cell membranes. Tumor cells lacking functional p53 would show lower elasticity and higher deformability [57],



and their membrane might be much more sensitive to a pulsed-wave ultrasound with a repetitive radiation pressure of a gradient around several Pa/mm during sonication. In Fig. 2-4, the pUH group exhibits a similar therapeutic response as the PLD alone group and this phenomenon might relate to the impact of pulsed-wave ultrasound on the sonicated cancer cells. In addition, ultrasound sonication may affect the cell cycle progression temporarily at early time points (first 12 h post sonication) and then diminish by 24 h [58]. In this study, *in vitro* experimental results (Fig. 2-3) and *in vivo* experimental results (Fig. 2-6, Fig. 2-7) demonstrated that pulsed-wave ultrasound has an additional mechanical effect on the cancer cell membrane to result in a better accumulation of PLD in the sonicated cancer cells and tumor tissues than conventional continuous-wave ultrasound. The above causes might be the reasons of the better therapeutic efficacy for pUH than cUH under the same acoustic power and sonication duration.

Doxorubicin concentrations in tumor and normal brain tissues (Fig. 2-6) showed that there was no significant difference of PLD deposition in the sonicated normal brain tissues for both cUH and pUH. It is well-known that an intact blood-brain barrier prevents chemotherapeutics entering the parenchyma, and in this study the maximum temperature rise ($\sim 43\text{ }^{\circ}\text{C}$) and the resulting thermal dose ($\text{CEM}_{43^{\circ}\text{C}} < 2\text{ min}$) for both cUH and pUH were much lower than the threshold values ($48\text{ }^{\circ}\text{C}$, $\text{CEM}_{43^{\circ}\text{C}} = 12.8\text{ min}$) for thermally induced blood-brain barrier disruption and brain tissue damage [59]. Hence, this type of low thermal dose ultrasound sonication would not produce any damage to the normal brain tissues or increase nanodrug delivery into the sonicated normal brain tissues. On the other hand, the BTB/BBB in the brain tumor tissue is partially leaky due to the invading of tumor cells into the brain parenchyma to alter vascular permeability. As the brain tumor grows, the enhanced permeability and

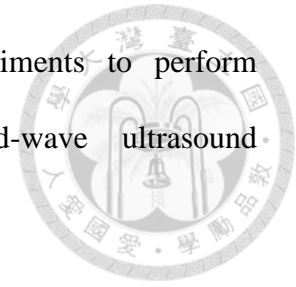


retention (EPR) effect occurs but this effect in brain tumors is still weak. Ultrasound hyperthermia can locally increase the sonicated brain tumor temperature, leading to increased perfusion, vascular permeability, and interstitial micro-convection in the heated tumor region; and hence both cUH and pUH have an enhanced PLD deposition in the sonicated tumor region. In this study, the experimental results further demonstrated that pulsed-wave ultrasound hyperthermia not only could heat brain tumors but also could make BTB more permeable for the PLD delivery into the sonicated tumors to achieve a significantly better therapeutic efficacy.

2.5. Conclusions

The blood-brain barrier/blood-tumor barrier (BBB/BTB) is an obstacle for the delivery of chemotherapeutic agents to the brain tumor. In this study, both *in vitro* and *in vivo* experimental results demonstrated that pulsed-wave ultrasound and low-dose ultrasound hyperthermia could significantly enhance the PLD delivery into the sonicated cancer cells and tumor tissues than conventional continuous-wave ultrasound and ultrasound hyperthermia under the same acoustic power and sonication duration without damaging normal brain tissues. The results indicate that this pulsed-wave ultrasound hyperthermia technology can be very useful in delivering nanodrugs for the treatment of various types of brain cancer tumors.

Table 2-1. Ultrasound parameters used in the *in vivo* experiments to perform continuous-wave ultrasound hyperthermia (cUH) or pulsed-wave ultrasound hyperthermia (pUH).



	Continuous-wave Ultrasound Hyperthermia (cUH)	Pulsed-wave Ultrasound Hyperthermia (pUH)
Frequency (MHz)	0.5	0.5
Peak Negative Pressure (MPa)	0.97	1.37
Pulse Repetition Frequency (Hz)	N/A	1000
Duty Cycle (%)	100	50
Duration (min)	10	10
Acoustic Power (W)	2.22	2.22

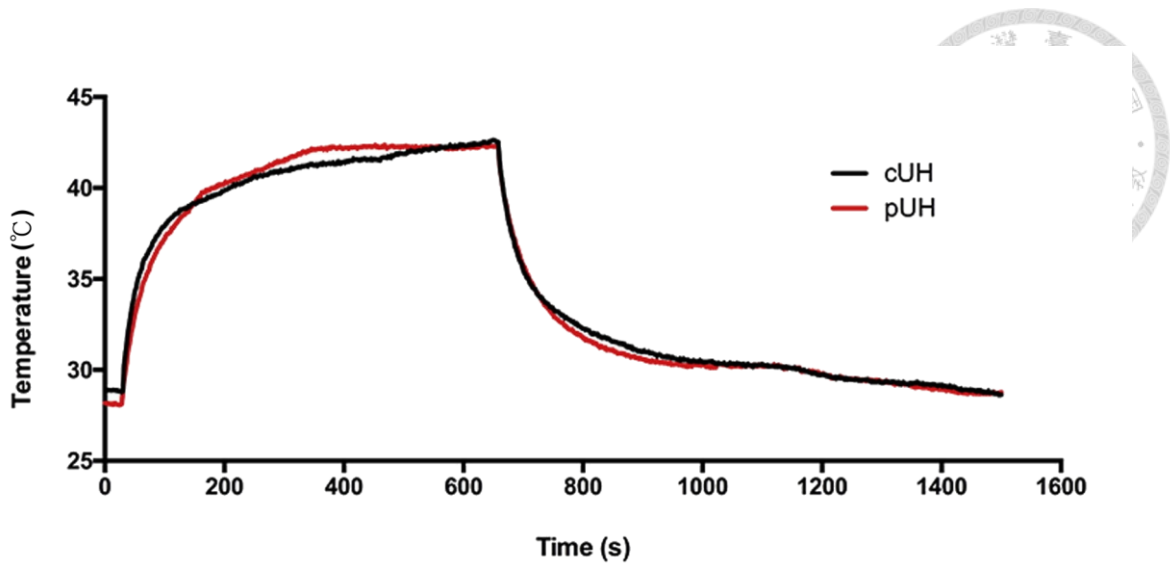


Figure 2-1. Typical temperature responses were measured at the focal zone with continuous wave or pulsed wave ultrasound sonication over time.

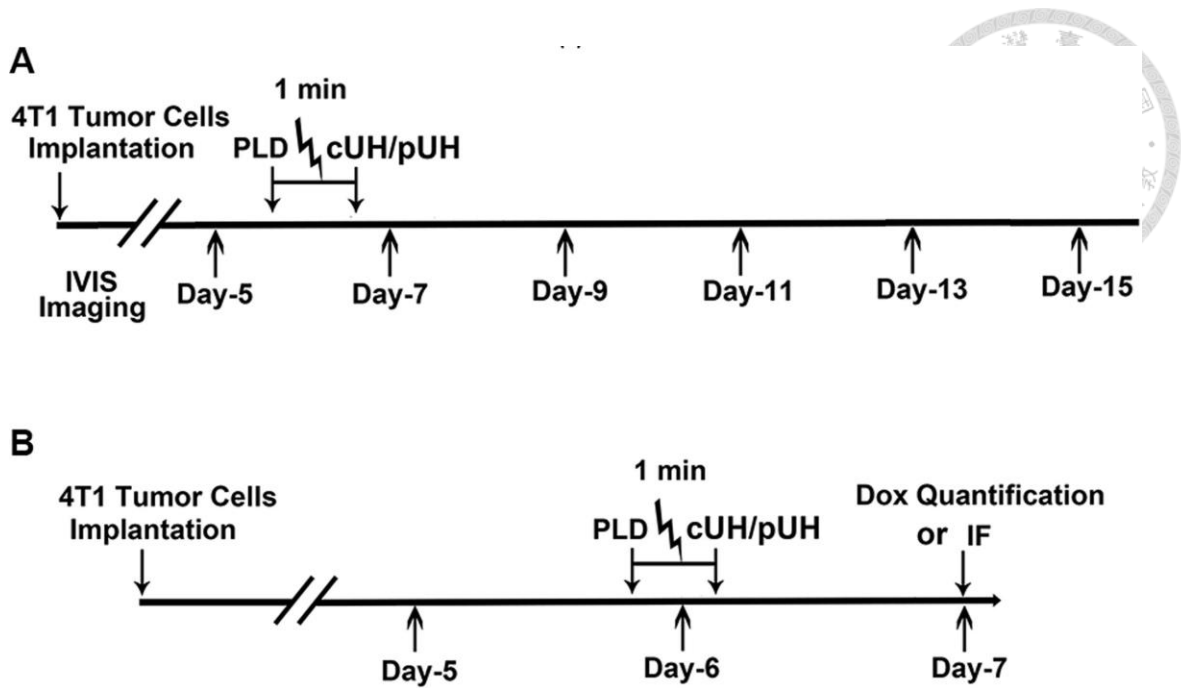


Figure 2-2. (A) Time course for the therapeutic experiments. 4T1 cancer cells were implanted on day 0, and the treatments were performed on day 6 with PLD injection, and/or continuous-wave ultrasound hyperthermia (cUH) or pulsed-wave ultrasound hyperthermia (pUH). IVIS imaging was performed on day 5, 7, 9, 11, 13 and 15. (B) Schedule for doxorubicin (Dox) quantification or immunofluorescence (IF) after different therapeutics.

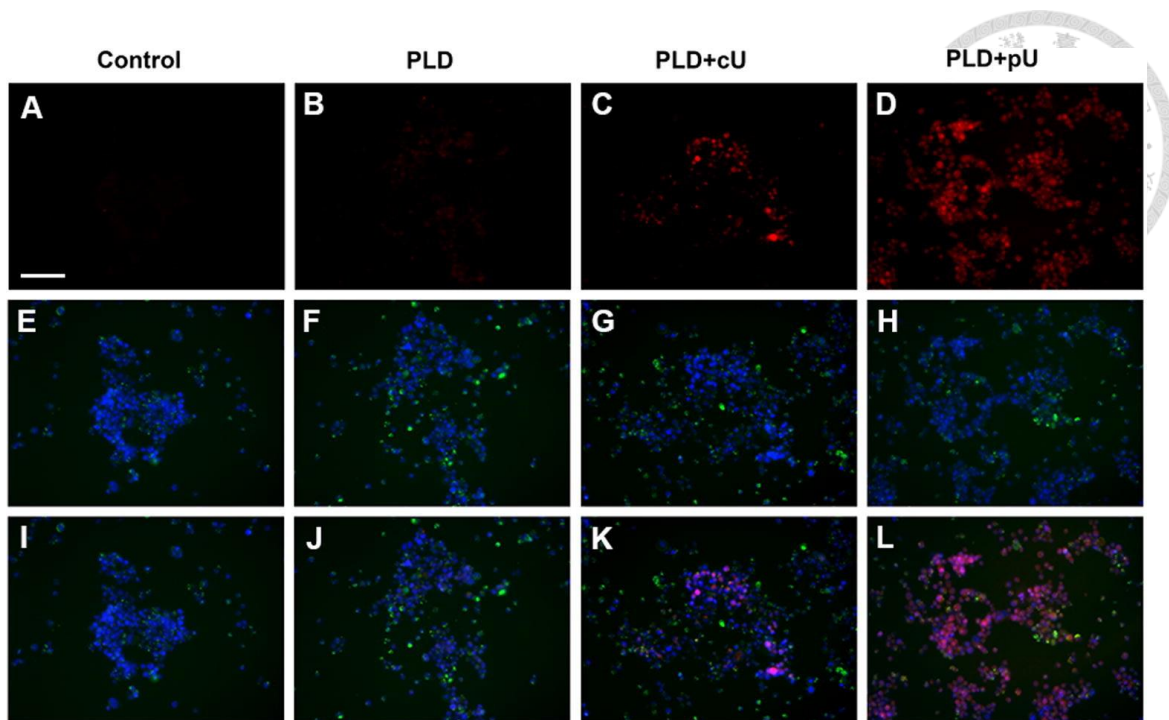


Figure 2-3. Immunofluorescence staining for *in vitro* investigation of PEGylated liposomal doxorubicin (PLD) up-taken by 4T1 breast tumor cells with or without ultrasound sonication. Fluorescence staining of tumor cells was performed 2 h after different therapeutics: 1) control: no treatment; 2) PLD: PLD alone; 3) PLD + cU: PLD plus continuous-wave ultrasound sonication; 4) PLD + pU: PLD plus pulsed-wave ultrasound sonication. A dose of 3 $\mu\text{g}/\text{ml}$ PLD was used in this experiment and the sonication duration was 3 min for both continuous- and pulsed-wave ultrasound with the same acoustic power (0.4 W). Red, blue and green colors represent PLD, cell nuclei and cell membrane, respectively. Scale bar = 200 μm .

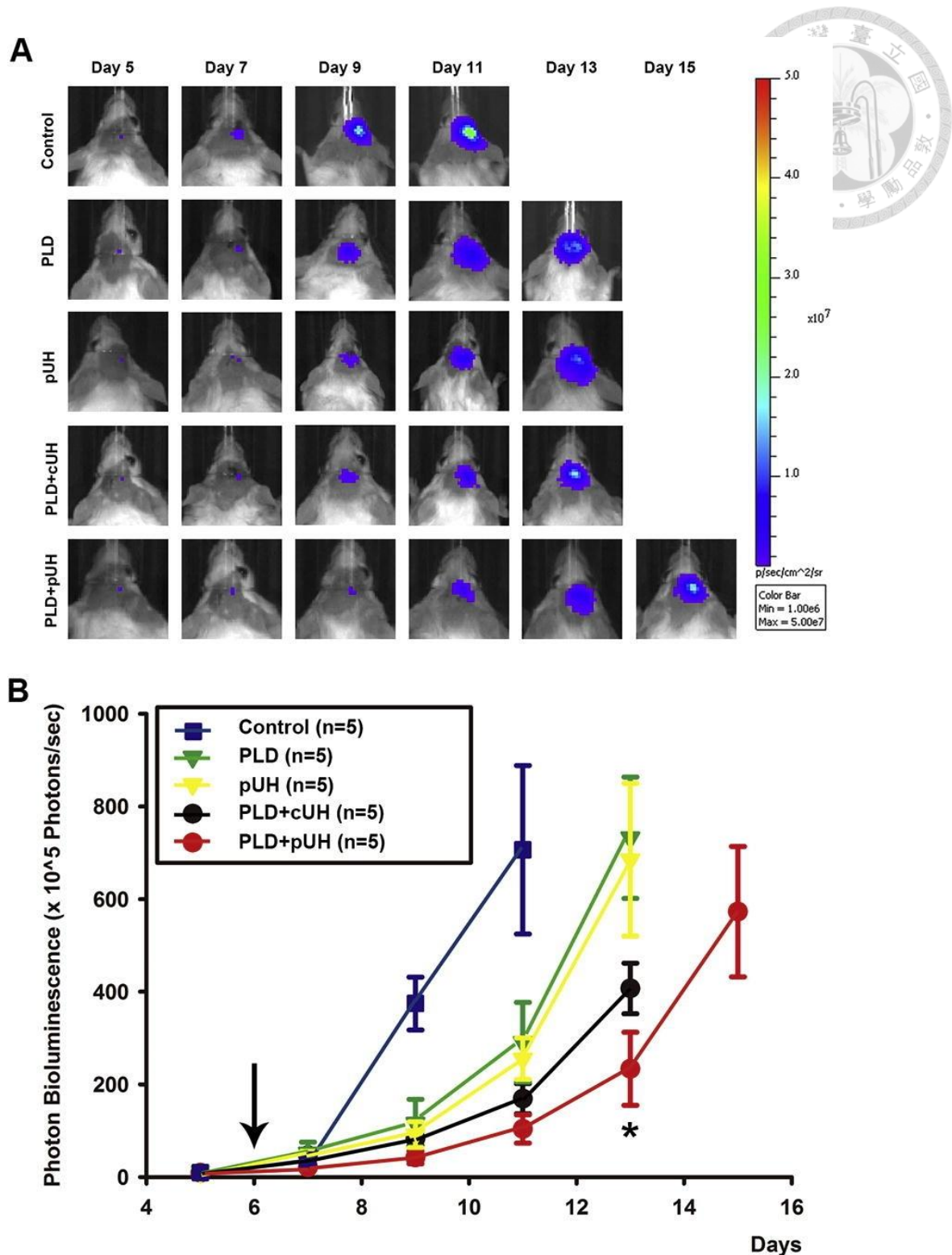
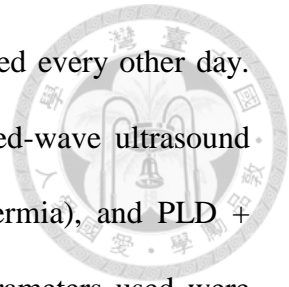


Figure 2-4. (A) Representative IVIS imaging and (B) bioluminescent signal quantification of mouse brain tumors from day 5 to day 15 after tumor implanted. Mice were implanted with luciferase-expressing 4T1-luc2 breast cancer cells in the brains. Bioluminescent signals were quantified using an IVIS imaging system. Treatment was

executed on day 6 after tumors implanted, and images were obtained every other day. There were five groups: Control (no treatment), PLD, pUH (pulsed-wave ultrasound hyperthermia), PLD + cUH (continuous-wave ultrasound hyperthermia), and PLD + pUH. A dose of 3.5 mg/kg PLD was used and the ultrasound parameters used were shown in Table 1. The arrow indicates the time point for different therapeutics performed. Note that PLD + pUH markedly inhibited the brain tumor growth. Data are presented as mean \pm SEM (n = 5 for each group). *Represents $p < 0.05$, the comparison between the PLD + pUH group and the PLD + cUH group.



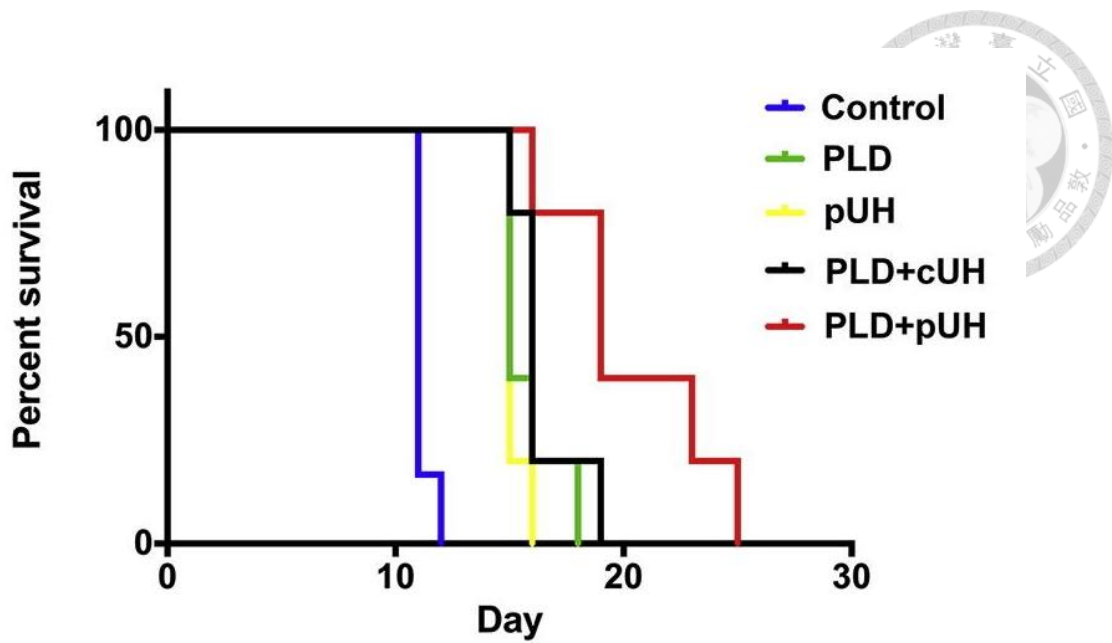


Figure 2-5. Kaplan-Meier survival curves of tumor-bearing mice with different therapeutics. PLD + pUH significantly increased the lifespan of tumor-bearing mice.

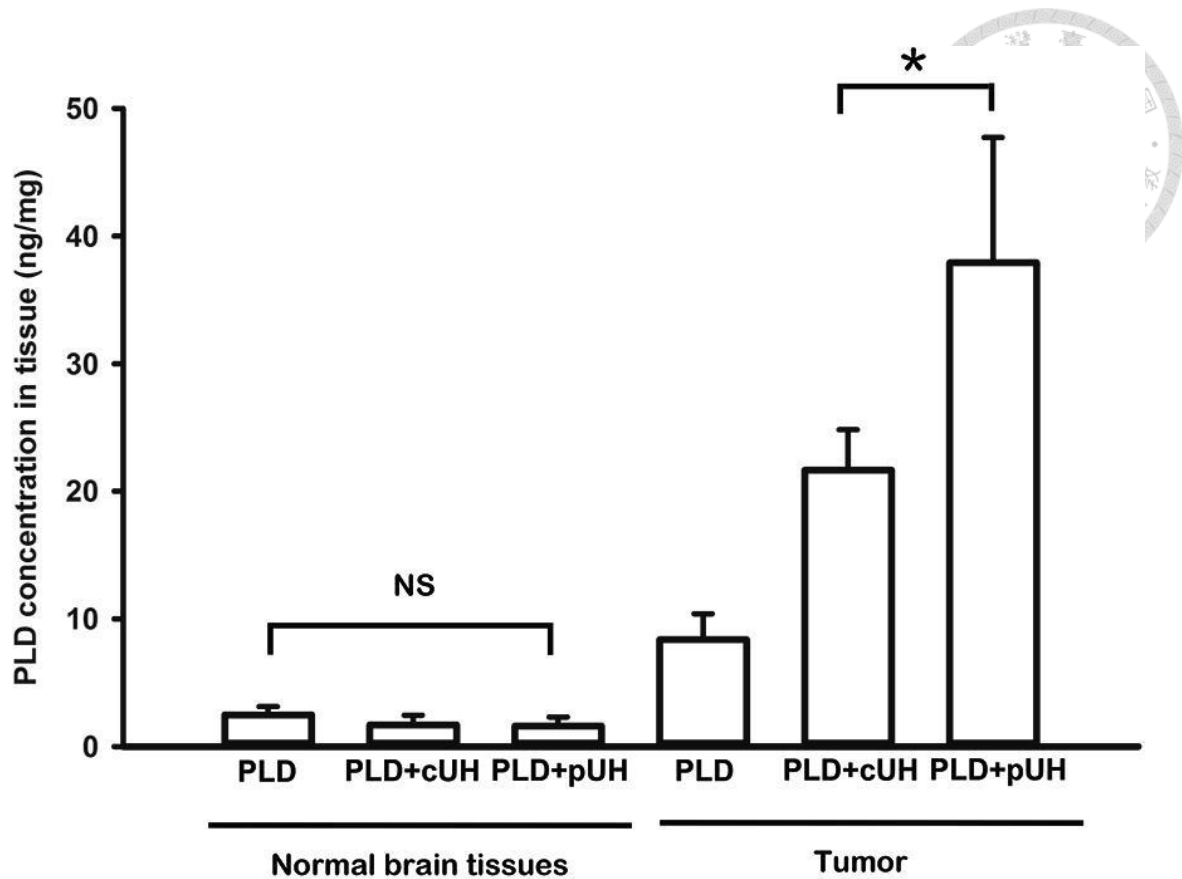


Figure 2-6. Doxorubicin concentrations in tumor and normal brain tissues for mice with/without continuous-wave ultrasound hyperthermia (cUH) or pulsed-wave ultrasound hyperthermia (pUH). Mice were implanted with 4T1-luc2 murine breast cancer cells on day 0 and were injected with a dose of 5 mg/kg PLD with/without transcranial cUH or pUH on day 6 after tumor implanted. Note that pUH significantly enhanced the accumulation of PLD in the tumor tissues than cUH. In addition, both cUH and pUH did not elevate the PLD concentration in the normal brain tissues. Data are presented as mean \pm SEM (n = 5 for each group). *Represents $p < 0.05$.

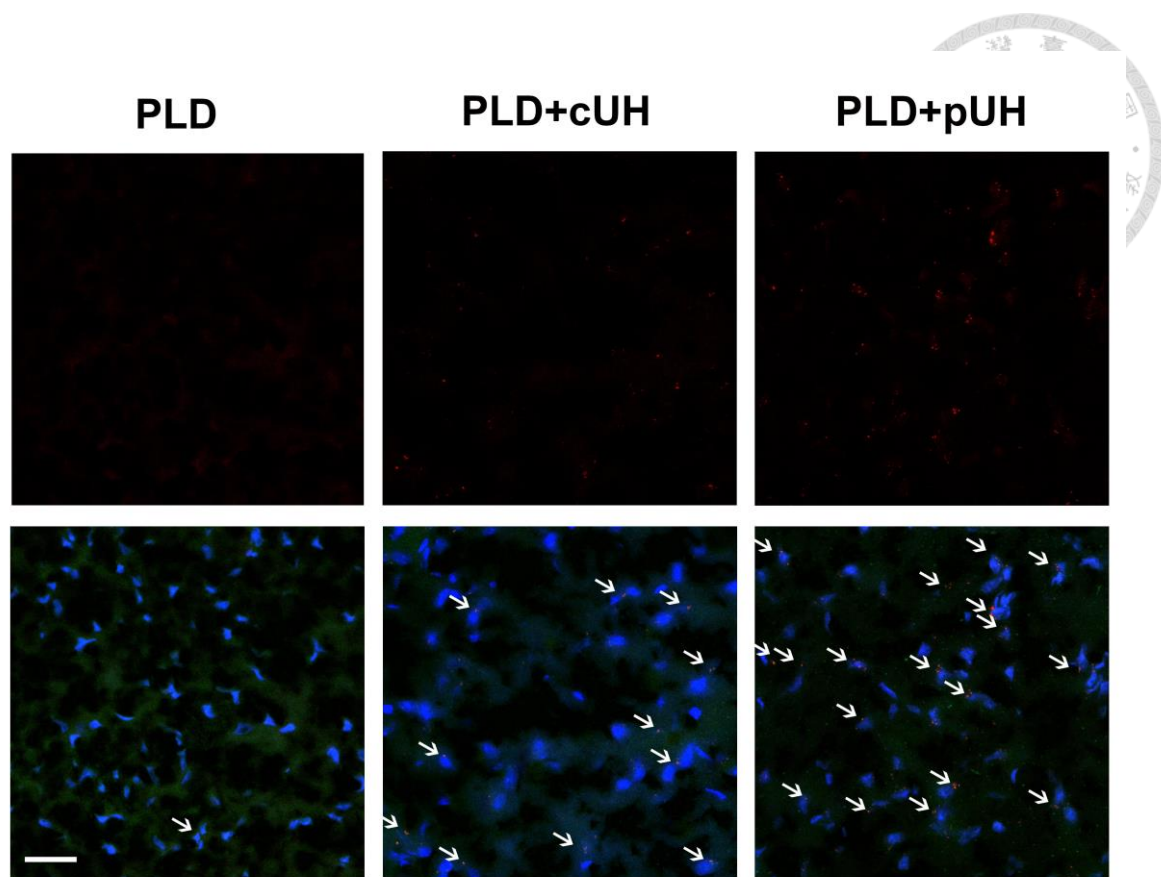


Figure 2-7. Immunofluorescence staining in the tumor regions after different therapeutics. Mouse brains were implanted with 4T1-luc2 tumor cells and the treatments were performed 6 days after tumors implanted. In these experiments, a dose of 15 mg/kg PLD was i.v. injected. The mice were sacrificed 24 h after the treatment and then the brain tissues were stained with DAPI to visualize the tumor cell nuclei (blue) and with PKH67 to show the cell membrane (green). Tumors treated with PLD + pUH had the strongest red fluorescence expression and the deposition of doxorubicin was near the cell nuclei. Scale bars: 50 μ m.

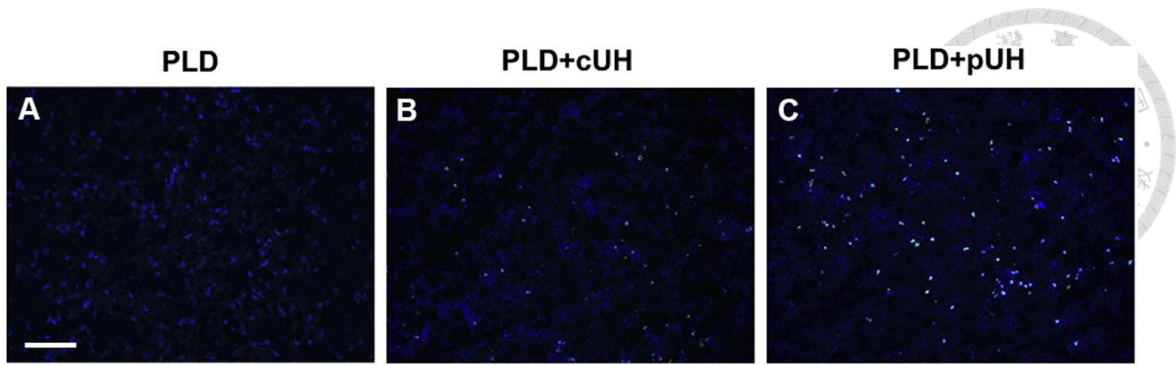


Figure 2-8. TUNEL staining was used to detect apoptotic cells in tumor tissues. Mouse brains were implanted with 4T1-luc2 tumor cells and the treatments were performed 6 days after tumors implanted. A dose of 3.5 mg/kg PLD was i.v. administered for these experiments. The mice were then sacrificed 24 h after the treatments and then brain tumor slices were obtained for staining. Tumor slices were firstly stained with terminal TUNEL (green) and then with DAPI to visualize the tumor cell nuclei (blue). The strong apoptotic signal was observed in the PLD + pUH group. Scale bar: 100 μ m.

Chapter 3. Pulsed-wave Ultrasound Hyperthermia Enhanced Nanodrug Delivery Combined with Chloroquine Exerts Effective Antitumor Response and Postpones Recurrence



3.1. Introduction

Autophagy is a catabolic process that turns over old proteins and organelles, allows cells to recycle cellular components and provides required energy [33,34]. It is a key component in maintaining homeostasis of cellular environment. Autophagy also plays a crucial role in cancer pathophysiology. It is believed that autophagy prevents cancer development, but helps cancer cells within an already established tumor to survive from stress and threats [33,34,35,36,37,38]. Therefore, autophagy inhibition has been investigated as an evolving strategy to fight against advanced cancer [37,38,39].

Chloroquine (CQ) and its analogue hydroxychloroquine (HCQ) are widely used anti-malarial drugs. They inhibit lysosomal acidification and hence block the formation of autophagosome as well [37]. In addition to autophagy inhibition, CQ was reported to possess multiple mechanisms to fight against cancer, including targeting against cancer stem cells (CSC) [40] and inducing tumor vessel normalization [41]. The link between CQ and cancer can be traced to 1980s, a malaria suppression program carried out in Tanzania utilizing CQ were found accompanied with a significant decline in Burkitt's lymphoma within the period of CQ distribution program [60]. There were several ongoing clinical trials using CQ (or HCQ) additional to conventional chemotherapeutic agents to treat various kinds of cancer, including colorectal cancer, glioblastoma, and pancreatic cancer [38].

Hyperthermia has been used to treat many kinds of cancer for decades, either

monotherapy or in combination with other anti-cancer therapy. The synergistic effect between hyperthermia and chemotherapeutic agents such as doxorubicin was well-known [15]. Furthermore, localized hyperthermia increases blood flow and vascular permeability in the heated tumor region, and therefore enhances the delivery of nanodrug into cancer cells [26]. Ultrasound was investigated as a modality to induce hyperthermia and was found advantageous over other thermal sources for its noninvasiveness and penetrating ability into deep tissues [25].

Previous studies [29,61] showed that short-time pulsed-wave ultrasound hyperthermia (pUH) not only enhanced the delivery of PLD but also elicited inhibitory effect directly on cancer cells. However, in some cases the cancer tumors were macroscopically destroyed by the combined therapy of PLD+pUH, they still recurred several days or weeks after the treatment.

The aim of present study was to investigate an effective strategy to successfully treat tumor, prevent tumor recurrence, and improve the disease-free survival. We evaluated the combination treatment of PLD+pUH with constant CQ administration to see if it successfully suppressed tumor growth and prevented recurrence. The concept of therapy and design of experiment was schemed in Figure 3-1 and Figure 3-2, respectively. We found that pUH enhanced PLD delivery in combination with CQ could persistently suppress 4T1 tumor growth and postpone its recurrence.



3.2. Materials and Methods

3.2.1. Chemical Reagents

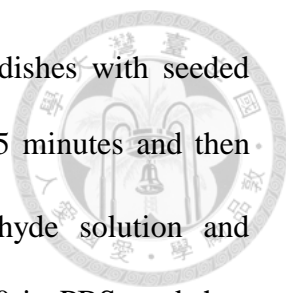
The PLD used in this study was a commercial product, Lipo-Dox® purchased from Taiwan Tung Yang Biopharm Company Ltd. It contains 2 mg/mL doxorubicin and 14 mol/mL phospholipids. The lipid composition is distearoylphosphatidylcholine, cholesterol, and PEG-DSPE with a molar ratio 3:2:0.3, respectively. The average particle diameter of the PLD determined by dynamic light scattering is 84.5 ± 18.6 nm at 37°C , with a narrow size distribution. The mean particle diameter, size distribution, and doxorubicin release rate were quite unaffected by temperature [62]. The elimination half-life of Lipo-Dox is about 65 h. Chloroquine (CQ) was purchased from Sigma-Aldrich.

3.2.2. Tumor cells

4T1 murine breast cancer cells (ATCC® CRL-2539TM) were cultured in Roswell Park Memorial Institute (RPMI) 1640 medium supplemented with 10% heat-inactivated fetal bovine serum (FBS) in 10 cm tissue culture dishes in a 5% CO₂-containing incubator at 37°C .

3.2.3. *In vitro* fluorescence assay of PLD internalization by 4T1 cells with or without CQ.

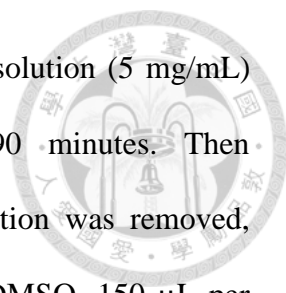
To elucidate if administration of CQ changed the distribution of PLD, we investigated if the hyperthermia-enhanced internalization of PLD was influenced by the presence of CQ. 4T1 murine breast cancer cells were seeded onto slide glasses (placed in 10-cm culture dish), supplied with RPMI 1640 medium containing 10% fetal bovine serum, and incubated for 24 hours. Then culture medium containing PLD solutions



(0.01 mg/mL) with/without CQ (10 μ M) were added into culture dishes with seeded slides. Dishes with slides were immersed in 43 $^{\circ}$ C water bath for 5 minutes and then incubated for 48 hours. Slides were fixed with 4% formaldehyde solution and permeabilized with 20 μ g/mL proteinase K and 0.2% Triton X-100 in PBS, and then stained with a solution containing Hoechst 33342 dye and mounted. Fluorescence images were obtained using a confocal microscope (AxioImager M1; Carl Zeiss Ltd., Oberkochen, Germany). Doxorubicin fluorescent detection was carried out with a green excitation/red emission filter, and blue channel for locating cell nuclei, respectively. All images were captured using the same exposure time. The pictures were merged using AxioVision Rel. 4.8 software (Carl Zeiss Ltd., Oberkochen, Germany). The fluorescent intensity of doxorubicin within nucleus regions depicted by Hoechst 33342 stain was measured and analyzed with ImageJ software. The mean fluorescent intensity was derived by dividing measured fluorescence with nucleus regions area. For the sake of statistical analysis, five representative fields were selected from each slide for the calculation of mean fluorescent intensity.

3.2.4. MTT Cytotoxicity Assay

MTT cytotoxicity assay was used to analyze the cytotoxic effect of different treatment on cancer cells. 4T1 murine breast cancer cells were seeded on a 96-well plate at a density of 2.5×10^3 cells/well, supplied with 100 μ L RPMI 1640 medium containing 10% fetal bovine serum. After 24 hours incubation, the cells were subjected to assigned treatment conditions. The concentration of PLD ranged from 0.02 mg/mL to 1 mg/mL. The concentration of CQ was 10 μ M. Hyperthermia was carried out with 43 $^{\circ}$ C water bath for 5 minutes. Cells incubated without any treatment were used as the blank control group. After 48 hours of treatment, old drug-containing medium was removed,



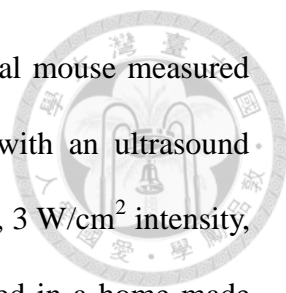
and 3-(4,5-dimethylthiazol-2-yl)-2,5-diphenyl tetrazolium bromide solution (5 mg/mL) was added (40 μ L per well) and incubated for further 90 minutes. Then 3-(4,5-dimethylthiazol-2-yl)-2,5-diphenyl tetrazolium bromide solution was removed, and precipitated crystals were dissolved with dimethylsulfoxide (DMSO, 150 μ L per well). The absorbance values were determined with a microplate reader (Synergy HTX; BioTek Instruments Inc., Winooski, VT, USA) at a wavelength of 540 nm.

3.2.5. *In vivo* tumor model

All animal experiments were approved by the Institution of Animal Care and Use Committee of College of Medicine in National Taiwan University. All procedures regarding animal experiment were conducted in accordance to relevant guidelines and regulations. Eight-week-old female BALB/c mice were acquired from BioLASCO Taiwan Co., Ltd. and were housed with a 12-h light/dark cycle and allowed free access to water and standard diet. The mice were anesthetized by 1–3% isoflurane inhalation during the tumor implantation procedure. The hair on right flank was shaved before tumor implantation. A total of 10^6 4T1 tumor cells suspended in 100 μ L of phosphate buffered saline (PBS) were slowly injected subcutaneously into the right flank of the mice.

3.2.6. Animal treatment experiment

The time schedule of treatment experiment was summarized in Figure 3-2. Five days after tumor implantation, the tumor volume reached about 100 mm³ and the treatment started. The tumor-bearing mice were randomly assigned to one of the following four groups: PLD+pUH+CQ, PLD+pUH, CQ, and Control. PLD solution was diluted with normal saline (1:1 volume ratio) and then injected via tail vein with a dose



of 10 mg/kg body weight according to the body weight of individual mouse measured right before the treatment. Ten minutes later, pUH was applied with an ultrasound sonicator (US-700; ITO, Japan) at 1 MHz frequency, 50% duty cycle, 3 W/cm² intensity, and 15 min sonication duration. The ultrasound probe was immersed in a home-made water bag filled with degassed water, and the water bag was mounted onto the tumor to prevent skin burn during ultrasound hyperthermia. CQ (dose 50 mg/kg body weight, dissolved in drinking water) was given daily via oral gavage since Day 5. Mice were closely monitored for their health status, and tumors were measured with a digital caliper every three days. Tumor volume was estimated by $0.5 * \text{Length} * \text{Width}^2$.

3.2.7. Histopathological examination and immunohistochemical study

The mice were subcutaneously implanted with 10^7 4T1 murine breast cancer cells suspended in 100 μ L of PBS at right flank. Seven days later, the mice were divided into the following four groups: PLD+pUH+CQ, PLD+pUH, CQ, and Control, and then received treatment. The treatment procedures were similar to description in the Animal treatment experiment section, with following change: CQ was given daily via oral gavage with a dose of 100 mg/kg body weight. Three days after the treatment, the mice were euthanized and the tumors were harvested. The harvested tumors were cut into two halves. One was subjected to histopathological examinations, immunohistochemical studies, and TUNEL assay. The other was processed for Western blotting.

Halves of the harvested tumors were fixed in 4% paraformaldehyde solution for three days and then embedded in paraffin blocks and sliced. Tumor tissue sections were stained with hematoxylin-eosin (H&E) for histopathological examination. For immunohistochemical studies, tumor tissue sections were de-paraffined and rehydrated,

and then treated with Proteinase K in a 37°C incubator to retrieve antigens. After antigen retrieval, tissue sections were incubated with primary antibody against LC3B (1:500, CellSignaling, cat. No. 3868) overnight at 4°C. After several washes, tissue sections were incubated with Dako LSAB 2 system to label primary antibodies and counterstained with hematoxylin for greater contrast. After dehydration and mounting, the prepared tissue sections were examined with microscope.

3.2.8. TUNEL assay

Tumor tissue sections were processed for TUNEL assay using a DeadEnd Fluorometric TUNEL system (Promega, Madison, WI, USA) according to the manufacturer's instructions. In brief, tissue slides were fixed with 4% paraformaldehyde solution and permeabilized with 20 µg/mL proteinase K. The slides were then labeled with rTdT enzyme mixture overnight at 37°C. The slides were then stained with Hoechst 33342 dye and mounted. Fluorescence images were obtained using a confocal microscope (AxioImager M1; Carl Zeiss Ltd., Oberkochen, Germany), using the FITC channel for detecting apoptotic cells and DAPI channel (excitation at 340–380 nm and emission at 435–485 nm) for revealing cell nuclei, respectively. All images were captured using the same exposure time. The pictures were merged using AxioVision Rel. 4.8 software (Carl Zeiss Ltd., Oberkochen, Germany).

To quantitatively compare the difference of apoptosis activity among groups, five representative fields were picked from each slide, and the total fluorescent intensity in each field was measured with ImageJ software. Statistical significance was tested with Student t test.

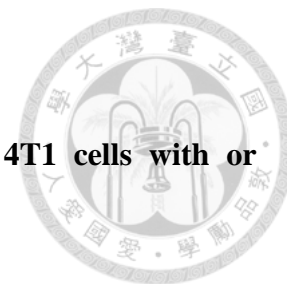
3.2.9. Western blotting

The tumor tissues were homogenized and purified with RIPA and then prepared with 6X SDS sample buffer. Equal aliquots of protein (30 μ g) were loaded onto 10% SDS-PAGE electrophoresis gels and run with 100 V for 60 min. The proteins were then transferred to nitrocellulose membranes with 100 V for 100 min. The membranes were then washed with TBST for several times and blocked for 60 min. After several washes, the membranes were cut into corresponding pieces and incubated with anti-LC3B antibody (1:1000, CellSignaling, cat. No. 3868), anti- β -actin antibody at 4°C overnight. After incubation, anti-LC3B antibodies were labeled by incubating with goat anti-rabbit HRP antibody (Santa Cruz) for 60 min at room temperature, whereas anti- β -actin antibodies were labeled by incubating with HRP goat anti-mouse antibody (BioLegend Cat. No. 405306). The expression of proteins was visualized with WesternBright™ ECL HRP substrate (Advansta Inc., CA, USA). The quantification of bands was performed with ImageJ software.

3.2.10. Statistical analysis

All numerical values were expressed in the form of mean \pm standard error of mean (SEM). The results were analyzed with two-way Student t test, and statistical significance was defined as $p < 0.05$. Analysis was performed with IBM SPSS Statistics version 20.0 (IBM Corp., Armonk, NY, USA).

3.3 Results



3.3.1. *In vitro* fluorescence assay of PLD internalization by 4T1 cells with or without CQ.

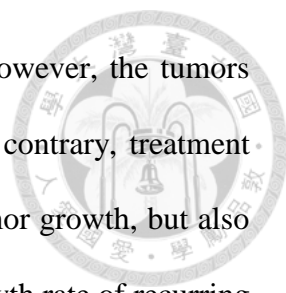
Figure 3-3A showed the fluorescent microscopic images revealing the distribution of doxorubicin (red) in PLD+CQ+H/PLD+H groups with respect to cell nuclei (blue). Figure 3-3B represented the mean fluorescent intensity in PLD+CQ+H/PLD+H groups. The mean fluorescent intensity in PLD+CQ+H group was slightly higher than that in PLD+H group, but the difference is small and statistically insignificant ($p=0.743$). It was concluded that CQ might enhance the transportation of PLD to nucleus, but this effect was unlikely to be a key factor underlying the extra anti-tumor efficacy of CQ.

3.3.2. MTT cytotoxicity assay

The cytotoxicity induced by different treatments was determined with MTT assay, and the result was represented in Figure 3-4. It was shown that treatment with PLD plus hyperthermia reduced cell viability in a dose-dependent fashion. By adding CQ, the cell viability was further reduced in all treatment conditions as compared to their corresponding counterparts without CQ. The differences were more remarkable in groups treated with no PLD and 0.04mg/mL PLD, but not in groups treated with higher dose of PLD (0.5 mg/mL and 1.0 mg/mL).

3.3.3. Combination treatment of PLD+pUH and CQ inhibited cancer tumor growth and delayed its recurrence

To investigate the effect of combination treatment of PLD+pUH with CQ, a single treatment of PLD+pUH was applied on 4T1 tumor-bearing mice on Day 5 followed by daily-given CQ. Figures 3-5B showed that tumor growth in PLD+pUH group was



inhibited, and the tumor shrank after the treatment since Day 5. However, the tumors treated with PLD+pUH were then relapsing since Day 17. On the contrary, treatment with PLD+pUH plus daily CQ administration not only inhibited tumor growth, but also drastically delayed tumor relapse until Day 32. Additionally, the growth rate of recurring tumors in the PLD+pUH+CQ group was much slower than that in the PLD+pUH group. Monotherapy with CQ alone had no benefit in inhibiting tumor growth as compared to the control group. All therapeutics were well tolerated, as neither significant drop in body weight nor apparent change in general activity was observed.

As shown in Figure 3-6, the survival rate of the PLD+pUH+CQ group seemed better than the PLD+pUH group. Up to Day 60, there were 6 among 8 treated mice achieved complete remission (defined by no observable tumor) in the PLD+pUH+CQ group, and 5 among 9 treated with PLD+pUH achieved complete remission. Nonetheless, the survival advantage of PLD+pUH+CQ group over PLD+pUH group did not reach statistical significance (p-value: 0.2). The survival of the CQ group did not differ from the control group, showing that CQ monotherapy had no significant benefit in suppressing tumor growth.

3.3.4. Immunohistochemical study proved autophagy of tumor cells blockaded by CQ administration

To investigate the change in tumor tissue affected by PLD+pUH+CQ treatment, tumor-bearing mice received single treatment of PLD+pUH on Day 7 after tumor implantation and were then fed daily with high dose CQ solution. Three days later, tumor were harvested and subjected to histopathological studies. H&E staining of tumor samples revealed that there was extensive necrosis in all groups (Figure 3-7). Some fat

cells surrounding the tumors or even infiltrating into tumor stroma could be observed. Figure 3-8, immunohistochemical staining, shows that LC3 expression (brown color) was markedly enhanced in both PLD+pUH+CQ and CQ groups, slightly increased in the PLD+pUH group, and nearly no expression in the control group. The results correlated well with the expected effect of CQ which inhibited autophagy and resulted in the accumulation of LC3-II.

3.3.5. TUNEL assay showed apoptosis increased by PLD+pUH, not by CQ

TUNEL assay was performed to assess the effects of different therapeutics on apoptosis of the treated tumors. Figure 3-9A showed that there were apparently stronger signals of apoptosis (green dots) in the PLD+pUH+CQ and PLD+pUH groups than those in the CQ and control groups, and the differences were highly significant (Figure 3-9B). The intensities of apoptosis signal were statistically similar in the CQ group and the control group. The difference between PLD+pUH+CQ group and PLD+pUH group was not significant as well. These results reflected that cancer cell apoptosis was induced by the treatment of PLD+pUH. Daily CQ administration did not alter the detectable density of cancer cell apoptosis, meaning CQ solely had no direct pro-apoptotic effect.

3.3.6. Western blotting

To demonstrate the autophagy inhibition induced by CQ, Western blotting assay was used to detect LC3 in tumor supernatant. Figure 3-10 showed the result of Western blotting targeting LC3. The expression of LC3-II was raised in the PLD+pUH+CQ and CQ groups, but not in the PLD+pUH and control groups. These findings coincided with the autophagy inhibition caused by CQ administration observed in

immunohistochemical stain.

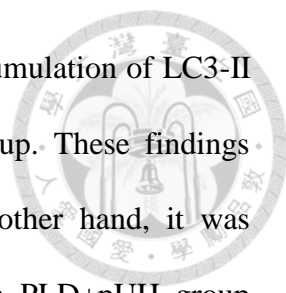


3.4 Discussion

Previous studies [29,61] showed that PLD in combination with pUH significantly inhibited the growth of 4T1 murine breast cancer in an *in vivo* brain metastatic tumor model. It was proved that pUH on the tumor after injection of PLD significantly increased the accumulation of PLD in the sonicated tumor tissue and cancer cells. Based on these results, we investigated if inhibition of tumor growth and tumor relapse could be further improved by combining PLD+pUH with CQ. To have a better observation, a subcutaneous tumor model was used instead. The experimental results shown in Figure 3-5 displayed that both PLD+pUH with and without CQ could successfully retard 4T1 tumor growth right after the treatment. Stronger retarding effect on tumor growth was obtained with the administration of CQ. The tumor inhibitory effect in the PLD+pUH group did not persist long, as the treated tumor began to grow again since Day 17. Treatment with PLD+pUH destroyed most cancer cells and resulted in tumor shrinkage, but still a small fraction of damaged cancer cells survived and regained the tumor growth several days after the treatment. The story tremendously differed in the case with PLD+pUH treatment followed by daily CQ administration. Treatment with PLD+pUH+CQ not only retarded cancer tumor growth more effectively, but also postponed the tumor regrowth until Day 32 and the regrowth rate of tumor was much slower as compared with the PLD+pUH group. This significant difference suggested that CQ, by blocking the escape mechanism of autophagy, rendered the cancer cells damaged by PLD+pUH treatment more difficult to survive. The prolonged retardation on tumor growth resembled the results obtained by Hirsch et al. [63,64], in which they showed metformin preferentially targeted CSC and exerted long-term inhibitory effect

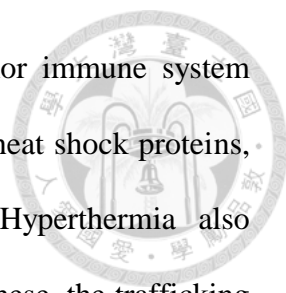
when co-administered with doxorubicin. It implied that the recurrence-postponing effect of CQ observed in our study might be partially attributed to similar anti-CSC activity.

Several researchers claimed that CQ potentiates anti-cancer therapeutics through mechanisms outside autophagy inhibition. Maes et al. found that CQ normalized tumor vessel structure, and the effect could not be mimicked by genetic inhibition of autophagy [41]. Balic et al. indicated that CQ suppressed CSC via inhibition of CXCR4 and Hedgehog signaling [40]. King et al. proposed that CQ synergized mTORi through mechanism related to cholesterol metabolism [65]. Nonetheless, the majority of researches still attributed the anti-tumor potency of CQ to its lysosomal acidifying/autophagy inhibition ability. Choi et al. concluded the anti-CSC activity of CQ was through autophagy inhibition despite their finding that Jak2-STAT3 pathway might also play a role [66]. Wei et al. showed in their study that autophagy inhibition rendered CSC susceptible to photodynamic therapy, regardless pharmacologic inhibition with CQ or genetic silencing [67]. Likewise, Lee et al. also found that CQ sensitized glioma cells to temozolomide, and the sensitizing effect was observed with other autophagy inhibitors as well [68]. They also demonstrated the sensitization by autophagy inhibition was p53 dependent. Similarly, Maycotte et al. identified certain subtypes of triple-negative breast cancer more responsive to autophagy-inhibiting treatment, and this susceptibility could be predicted by high STAT3 expression [69]. Furthermore, it is indicated that some activity of CQ shares the same underlying mechanism with autophagy inhibition: both are consequences of lysosome disruption. Elliot et al. found that lysosomal inhibition by CQ impaired de novo nucleotide biosynthesis and depleted aspartate in pancreatic ductal adenocarcinoma [70]. Even the aforementioned vessel-normalizing ability of CQ was proposed in a recent study to be related to lysosomal dysfunction [71].



In immunohistochemical studies and Western blotting, the accumulation of LC3-II was markedly increased in PLD+pUH+CQ group and in CQ group. These findings reflected the late-stage inhibition of autophagy by CQ. On the other hand, it was observed that the expression of LC3-II was slightly decreased in PLD+pUH group comparing to control group. Autophagy is usually induced by hyperthermic treatment as a response to protect cell from metabolic stress [72,73]. Nevertheless, there are controversy about how doxorubicin affects autophagy [74,75]. It is suggested that doxorubicin stimulates the initiation of autophagy but interferes the lysosomal function, therefore resulting in overall decrease in autophagy flux [75]. Park et al. demonstrated that doxorubicin reduces autophagosome formation via increase in mTOR expression [76]. The slightly reduced expression in LC3-II observed in PLD+pUH group could be explained by the summation of two opposite effects: upregulation by hyperthermia and downregulation by doxorubicin.

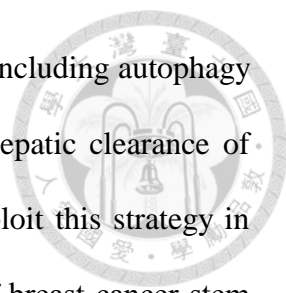
In our study, we used PLD+pUH to treat the tumors and employed CQ to prevent the remnant cancer cells escaping through autophagy. The results showed that when CQ used in combination with PLD+pUH, it assisted tumor suppression and postponed or even prevented tumor relapse. But CQ monotherapy has little impact on tumor growth as compared to the control group (as shown in Figure 3-5B). Autophagy works as a surviving mechanism when cancer cells face strong stresses. CQ blocks autophagy in cancer cells damaged by anti-tumor therapy, and therefore aggravates the severe condition remaining cancer cells confront, and eventually results in decreasing the probability of tumor relapse. However, this effect is not prominent by CQ monotherapy, and hence in the absence of antitumor therapeutics CQ does not alter tumor growth response.



Hyperthermia and CQ are both reported to activate anti-tumor immune system [12,77]. The expression of tumor antigens, including MHC class I, heat shock proteins, and exosomes, are observed in hyperthermia-treated tumors. Hyperthermia also stimulates NK cells, CD8⁺ T cells, and dendritic cells. Along with these, the trafficking of immune cells between lymphoid organs and tumor are improved [12]. CQ is shown to function as an anti-tumor immune modulator by resetting tumor-associated macrophages [77]. The immunomodulatory effects of hyperthermia and CQ may synergize each other and underlie the persistent suppression on tumor growth in our study.

The survival rate in the PLD+pUH+CQ group was better than that in the PLD+pUH group. Observed up to Day 60, the survival rate is 75% (6 among 8 treated mice) and 56% (5 among 9 treated mice) for the PLD+pUH+CQ group and the PLD+pUH group, respectively. There was no observable tumor (complete remission) for these surviving mice after the treatment of PLD+pUH with or without CQ. Despite the great success in achieving prolonged remission, the survival in the PLD+pUH+CQ group was not significantly better than PLD+pUH (p-value: 0.2). It might be due to that the therapeutic efficacy of PLD+pUH was sufficiently potent in suppressing tumor growth in the subcutaneous 4T1 tumor model, so the marginal benefit of adding CQ into treatment were harder to be demonstrated since PLD+pUH already had a good outcome. The difference of survival owing to CQ might be more apparent in a more lethal tumor model refractory to PLD+pUH treatment. The survival in CQ group was nearly identical to that in control group, consistent with the observation in tumor growth that CQ monotherapy had little benefit.

CQ in cooperation with nanomedicine has been suggested as a promising therapeutic strategy to treat cancer [78]. Pelt et al. highlighted in their review the



advantages of CQ to complement nanomedicine for cancer therapy, including autophagy inhibition, normalization of tumor vasculature, and reducing the hepatic clearance of nanoparticles [78]. There are increasing studies that practically exploit this strategy in cancer therapeutics. Sun et al. used CQ to reduce the ‘stemness’ of breast cancer stem cell to increase their susceptibility to chemotherapeutics such as doxorubicin and docetaxel [79]. Shao et al. designed a MPEG-PLA nanoparticle co-delivering CQ and doxorubicin to kill ovarian cancer, utilizing the lysosome-interfering property of CQ to hinder drug sequestration [80]. Wolfram et al. pretreated mice with CQ to reduce nanoparticle uptake by macrophage [81]. Lv et al. took advantage of the vessel-normalizing ability of CQ to improve microcirculation in tumor and promoted nanodrug delivery [82]. These studies demonstrated the versatile powerfulness of CQ in combination use with nanomedicine in cancer therapeutics. Our study further extended the strategy by adding pulsed-wave ultrasound hyperthermia, which assisted the delivery of nanodrug into tumor tissue and created a vicious microenvironment so that autophagy inhibition by CQ became crucial.

3.5 Conclusions

We demonstrated that pulsed-wave ultrasound hyperthermia (pUH) enhanced PLD delivery in combination with chloroquine (CQ) could persistently suppress 4T1 tumor growth and postpone its recurrence. These results may pave the way to develop new combinatorial strategy for treatment-refractory cancer.

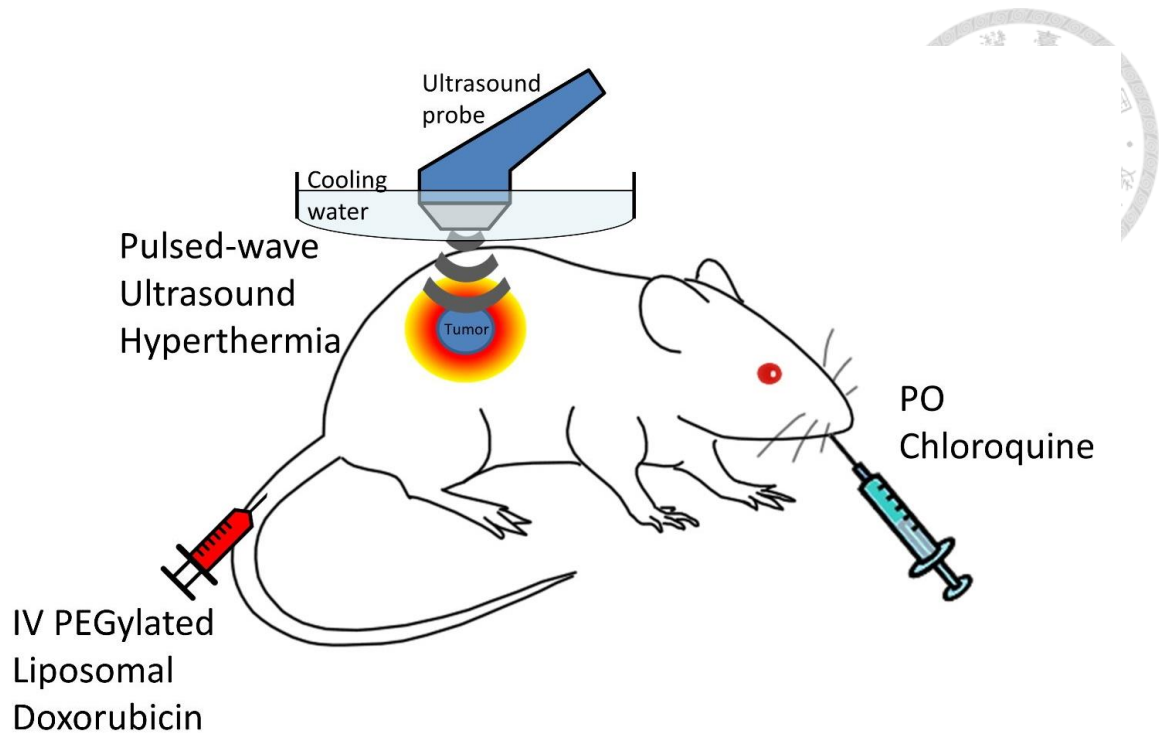


Figure 3-1. The scheme of PEGylated Liposomal Doxorubicin (PLD) + pulsed-wave Ultrasound Hyperthermia (pUH) + chloroquine (CQ) in cancer treatment.

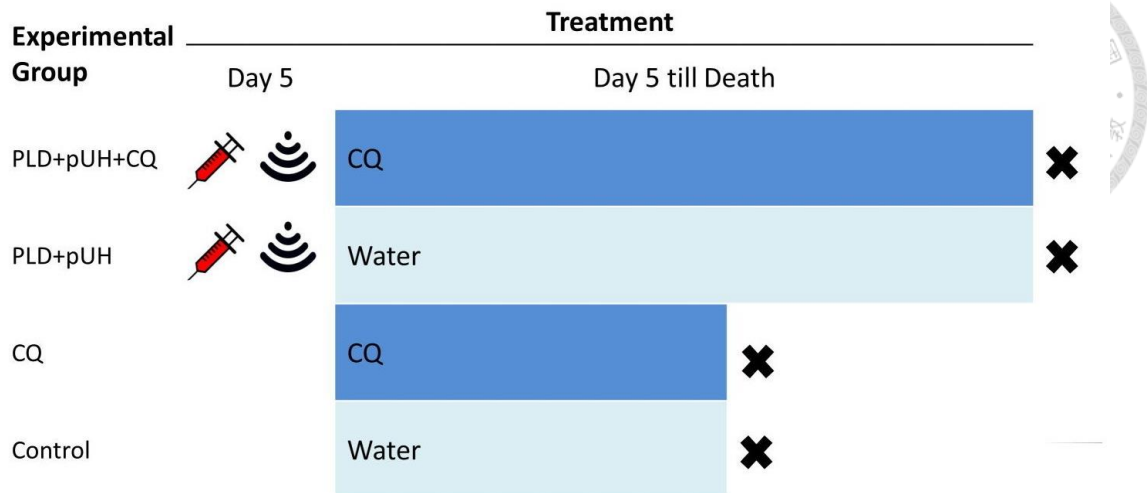


Figure 3-2. Time schedule of treatment experiment. PEGylated Liposomal Doxorubicin (PLD) was given intravenously on Day5 after tumor implantation. Pulsed-wave ultrasound hyperthermia (pUH) was administered 10~15 minutes after PLD administration. Then mice were orally fed chloroquine (CQ) dissolved in drink water daily till experiment end.

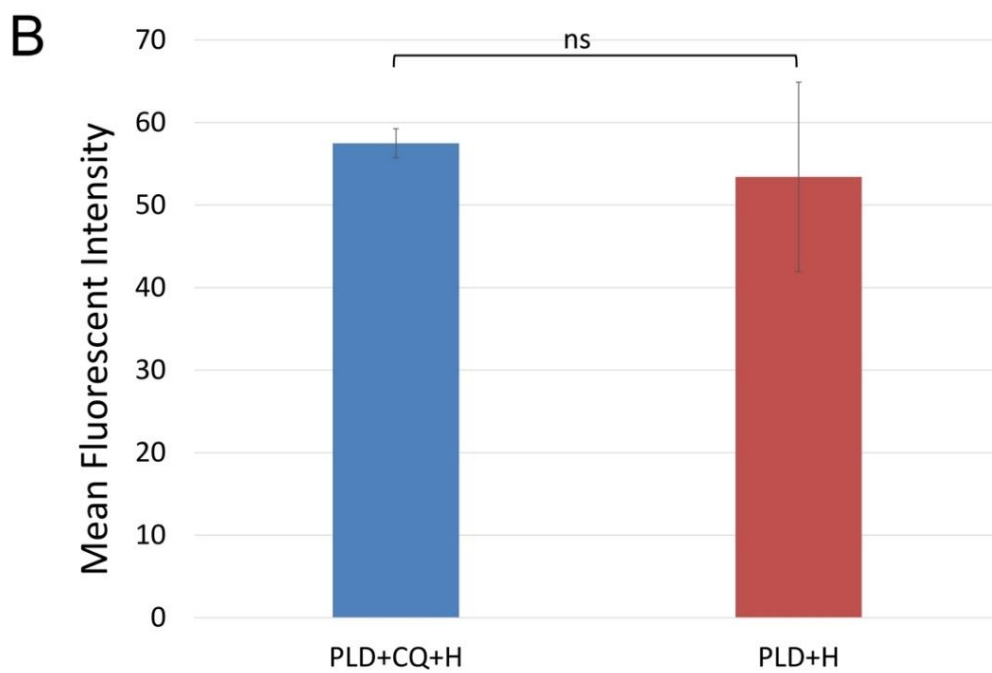
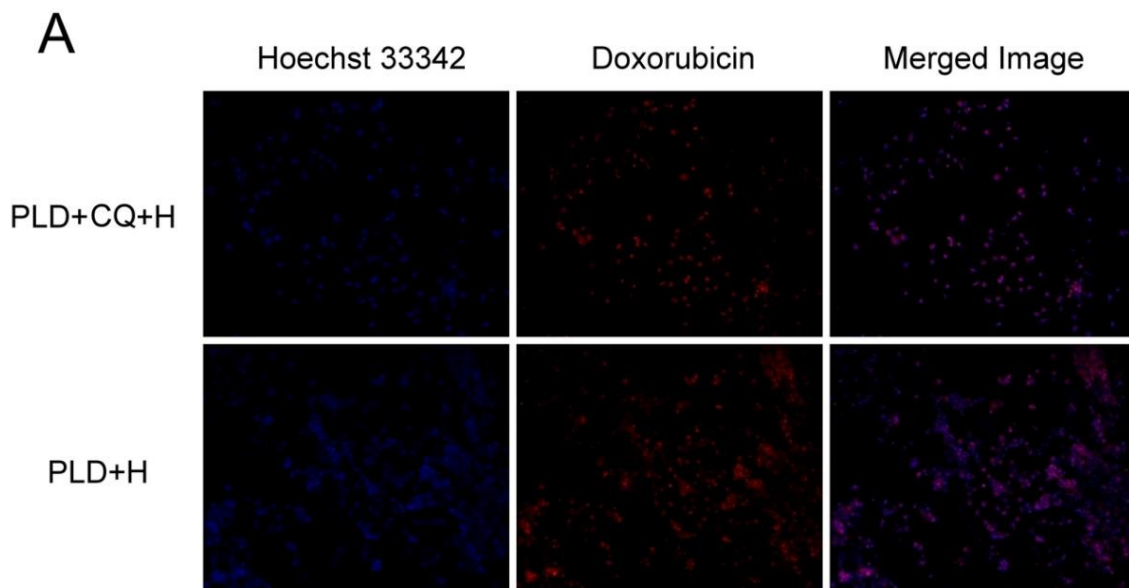


Figure 3-3. (A) Fluorescent microscopic images of 4T1 murine breast cancer cells *in vitro* treated with PLD+CQ+H or PLD+H. Doxorubicin (red) distribution with respect to nuclei (blue, stained with Hoechst 33342 dye) were shown. (B) Mean fluorescent intensity of doxorubicin with respect to nucleus region area. Abbreviation: H: hyperthermia. ns: not significant.

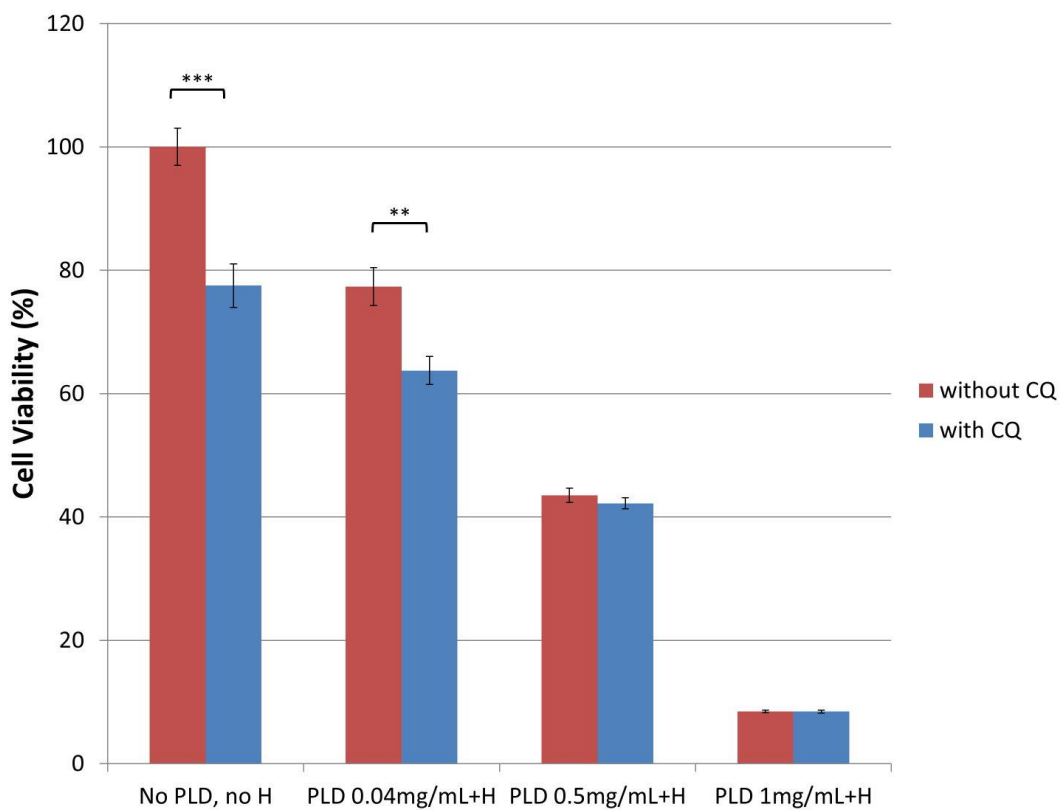
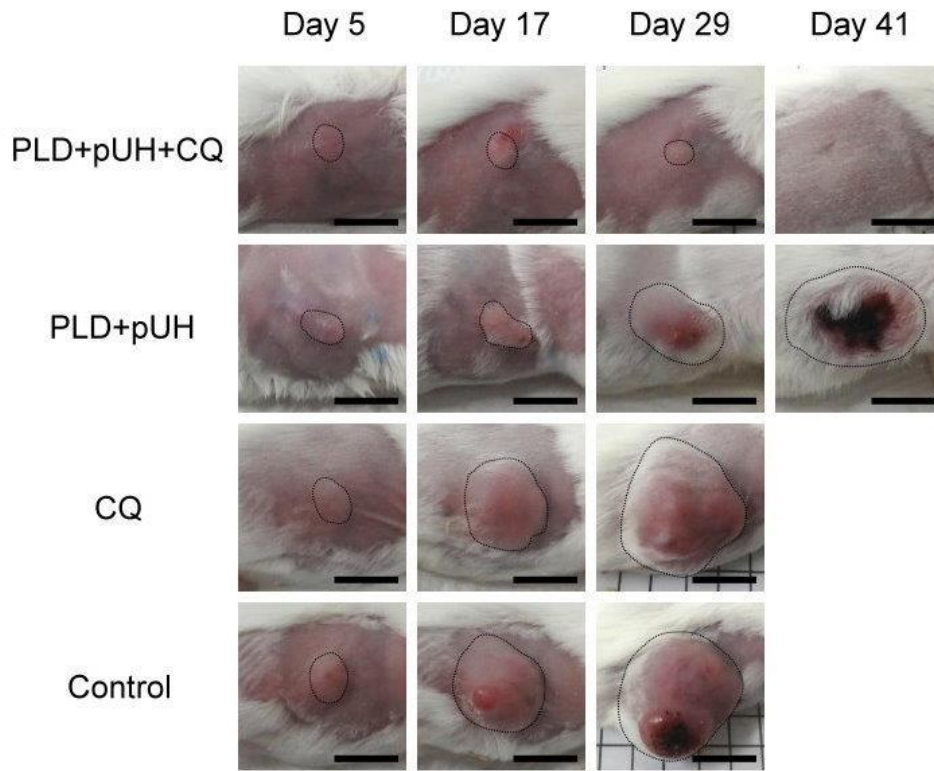


Figure 3-4. MTT Cytotoxicity Assay. The cell viability was reduced by PLD with hyperthermia in a dose-dependent manner. The addition of CQ (10 μ M) further potentiated the cytotoxicity of PLD+H comparing to the counterpart without CQ. **: p<0.01, ***: p<0.001. Abbreviation: H=hyperthermia

A



B

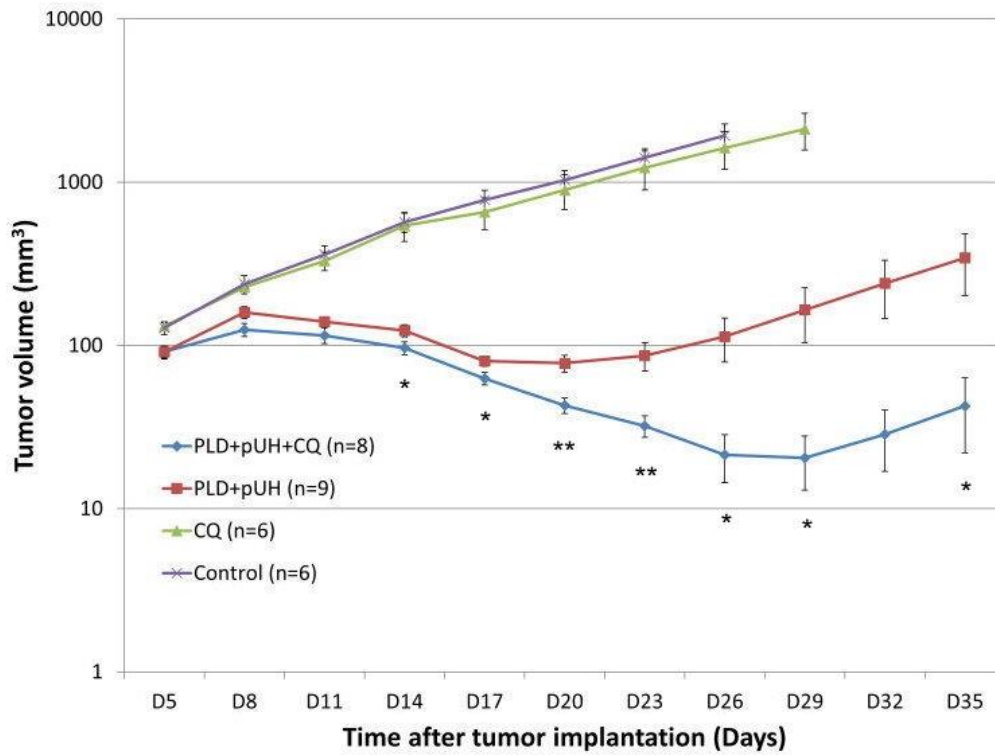
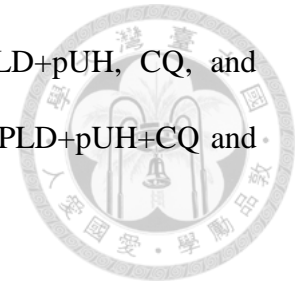


Figure 3-5. (A) Representative photographs of tumor for each group. Region encircled by dashed line indicated tumor. Scale bar=1cm. (B) The response of subcutaneous 4T1

murine breast cancer to different treatment: PLD+pUH+CQ, PLD+pUH, CQ, and control groups. * denotes $p < 0.05$, and ** denotes $p < 0.01$ between PLD+pUH+CQ and PLD+pUH, respectively.



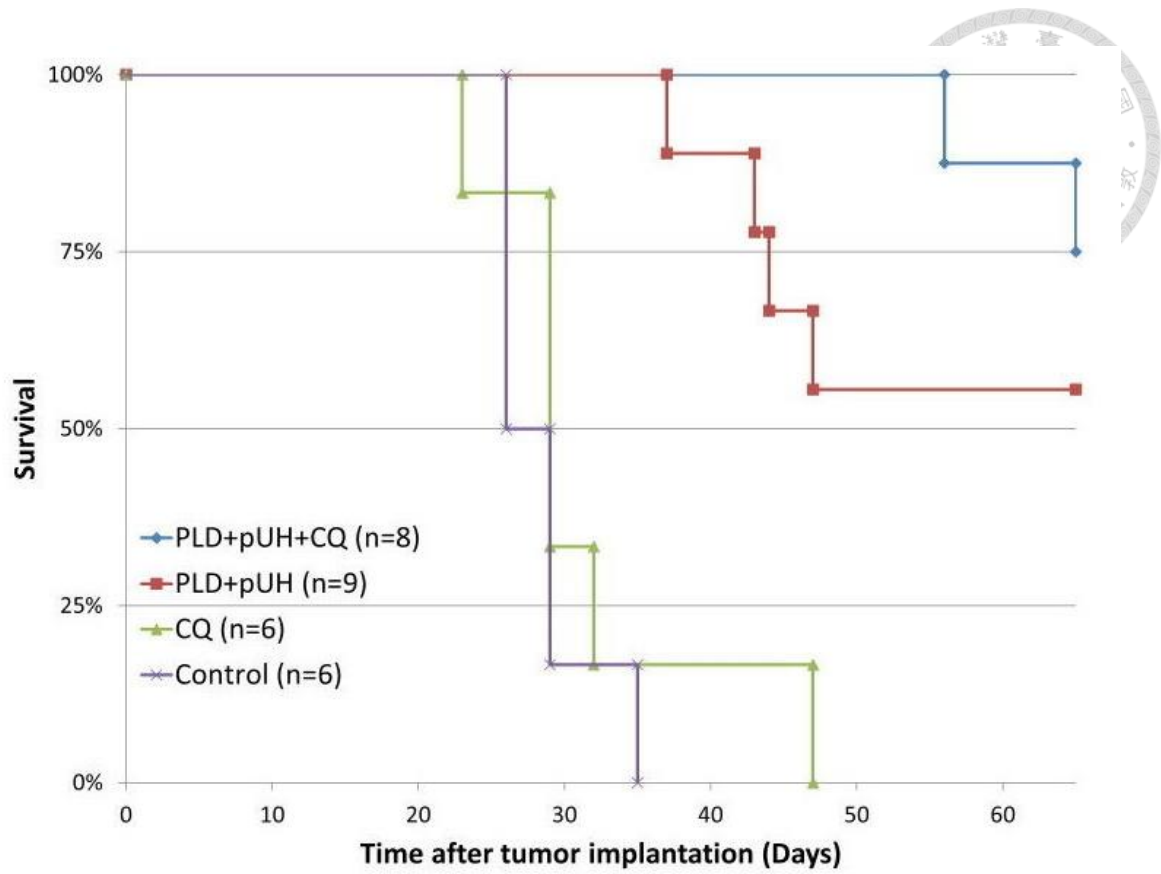


Figure 3-6. The Kaplan-Meier survival plot for PLD+pUH+CQ, PLD+pUH, CQ, and control groups.

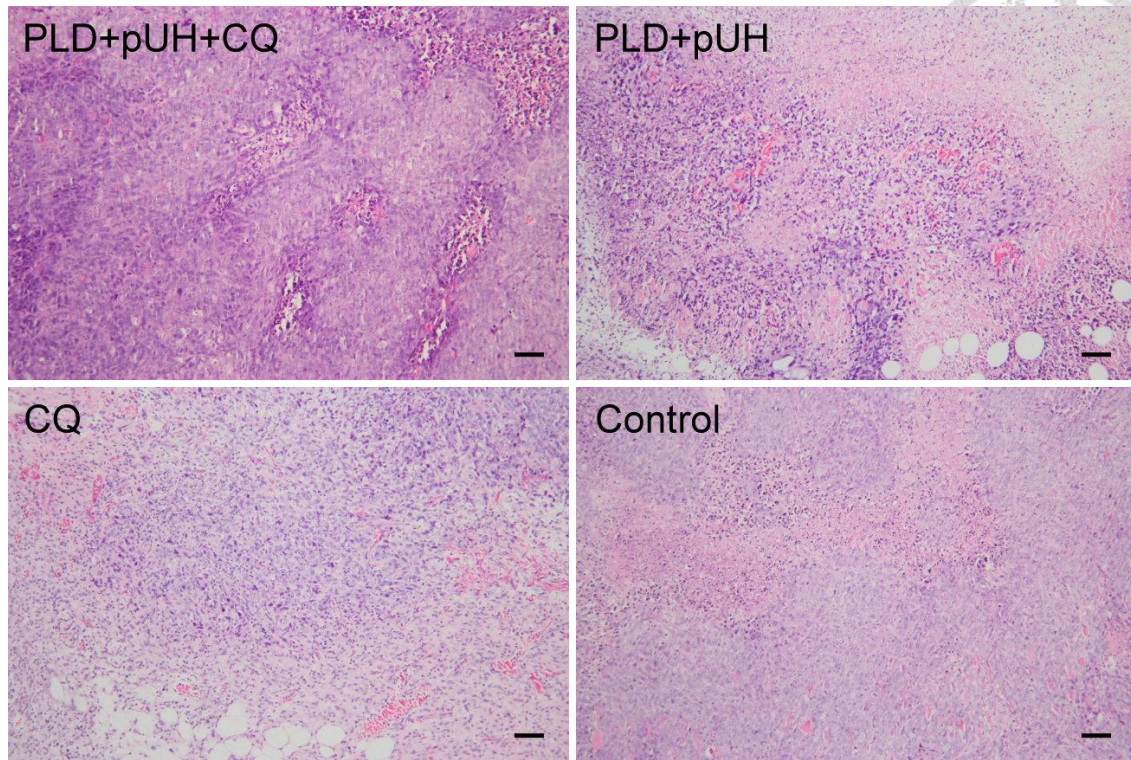


Figure 3-7. Histological examinations with hematoxylin-eosin staining for each experimental group. Scale bar = 100 μ m.

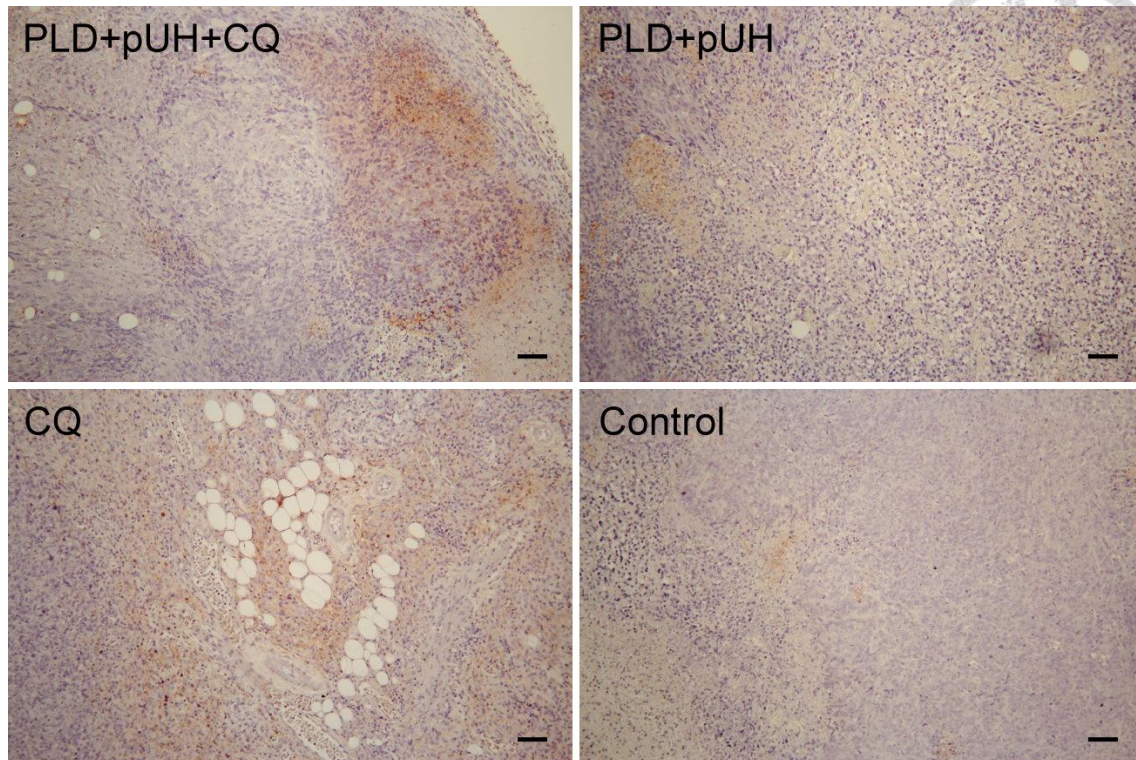
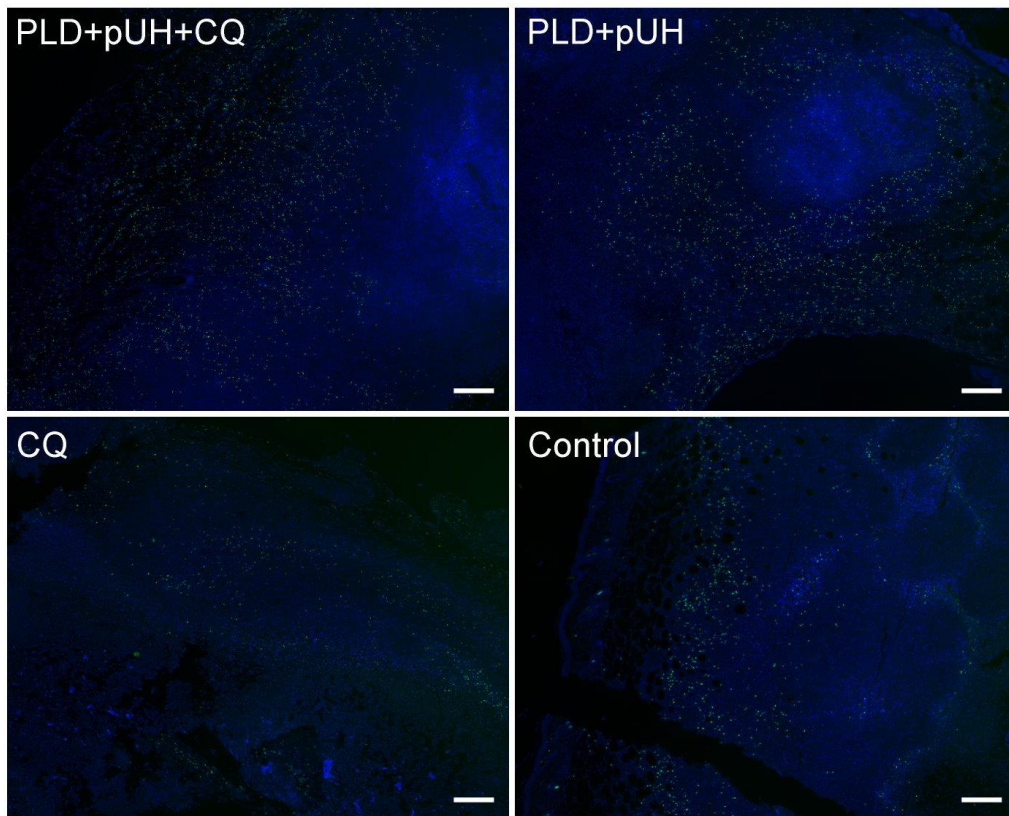


Figure 3-8. Immunohistochemical stain for LC3 (brown stain) for each experimental group. LC3 accumulation reflects late-stage inhibition of autophagy. Greatly increased accumulation of LC3 was observed in both PLD+pUH+CQ and CQ groups, whereas slightly increase in the PLD+pUH group, and nearly no accumulation in the control group. Scale bar = 100 μ m.

A



B

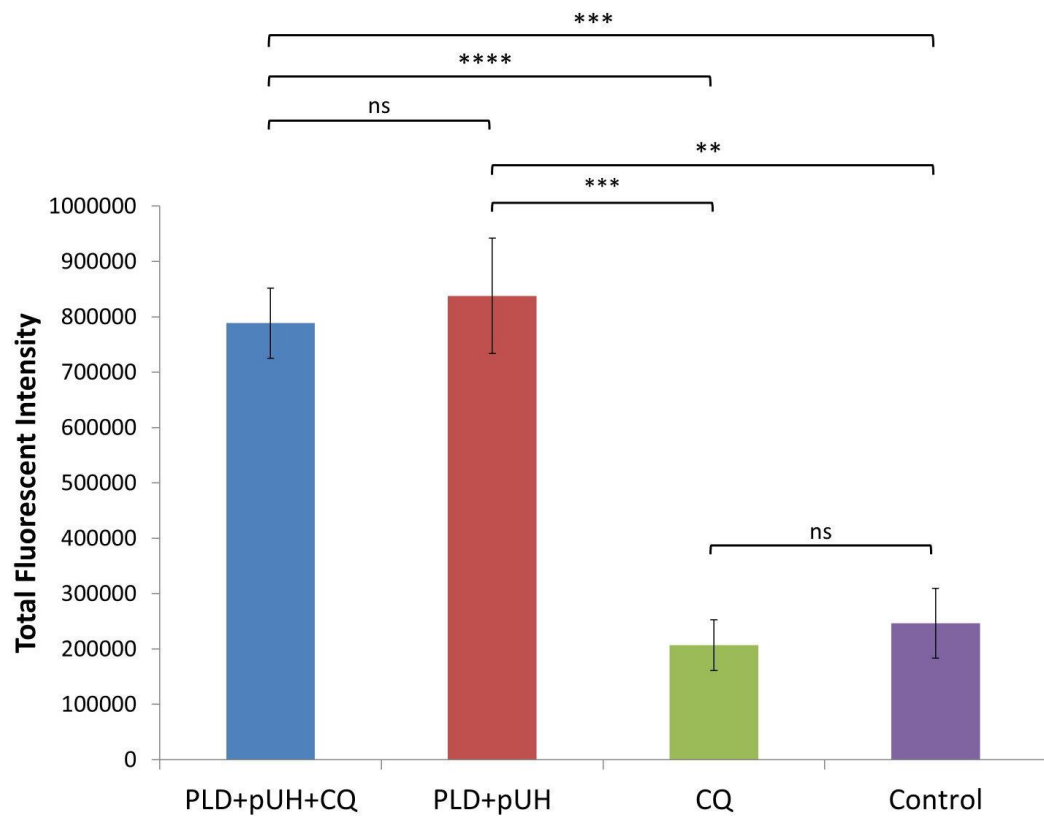


Figure 3-9. (A) Fluorescent microscopic images of TUNEL assay for each experimental

group. Apoptotic signals (green) were much more enhanced in PLD+pUH+CQ group and PLD+pUH group. Scale bar = 200 μ m. (B) The fluorescent intensities for each experimental group were quantified and analyzed for statistical significance. **: $p < 0.01$.

***: $p < 0.001$. ns: not significant.

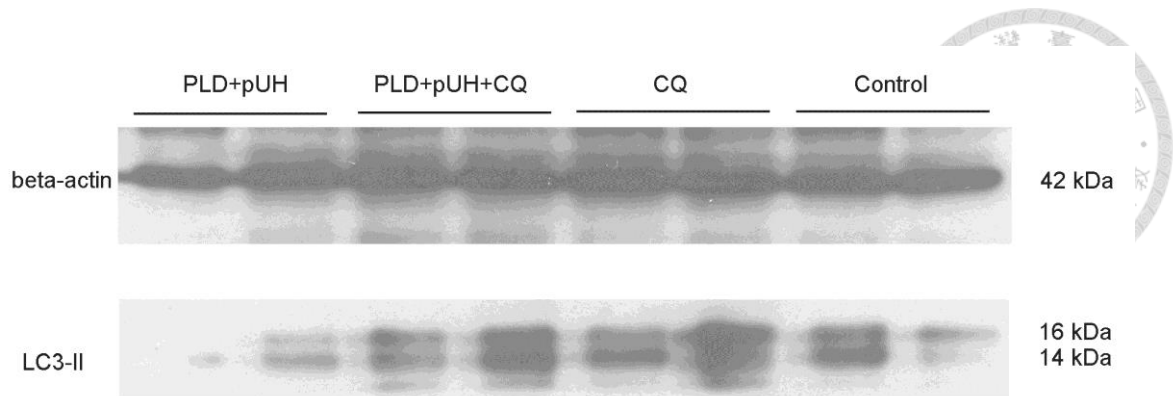


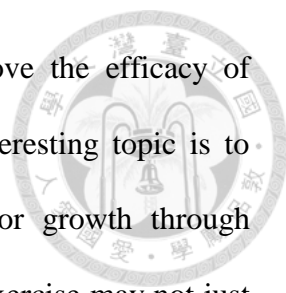
Figure 3-10. Western blot for LC3 for each experimental group. Increased expression of LC3-II was observed in PLD+pUH+CQ group and CQ group, reflecting the late-stage autophagy inhibition by CQ. LC3 expression was slightly reduced in PLD+pUH group comparing to control group.

Chapter 4. Summary and Future Work

In summary, we demonstrated that pulsed-wave ultrasound and low-dose ultrasound hyperthermia could significantly enhance the PLD delivery into the sonicated cancer cells and tumor tissues than conventional continuous-wave ultrasound and ultrasound hyperthermia under the same acoustic power and sonication duration without damaging normal brain tissues. The results indicate that this pulsed-wave ultrasound hyperthermia technology can be very useful in delivering nanodrugs for the treatment of various types of brain cancer tumors.

Furthermore, we proposed a novel treatment strategy by integrating pulsed-wave ultrasound hyperthermia enhanced delivery of PLD with constant chloroquine administration. We proved that this combinatorial strategy could persistently suppress 4T1 tumor growth and postpone its recurrence. These results may pave the way to develop new combinatorial strategy for treatment-refractory cancer. To the best of our knowledge, this is the first study to combine these elements into an integrated strategy to successfully treat cancer and prolong remission.

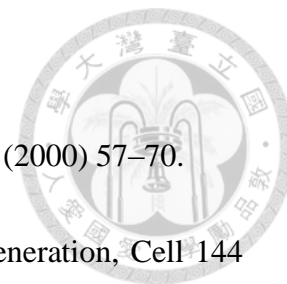
To push our research forward, we will generalize our treatment strategy of PLD+pUH+CQ to see if it works on different types of cancer. If it does or does not work, then we want to know what causes the distinct therapeutic response. We will also study the role of CQ in cancer therapeutics beyond autophagy inhibition. The multifaceted benefit of CQ, like vascular normalization, cancer stem cell inhibition, and decreasing nanoparticle clearance, will be assessed. With more knowledge about the actual efficacy of CQ, we can step further by combining our treatment strategy with other therapies. We may try the combination of PLD+pUH+CQ with immunotherapy. We anticipate the



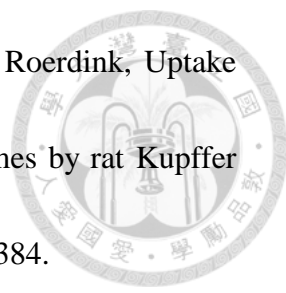
immunomodulation from CQ and pUH can synergistically improve the efficacy of immunotherapy, thus cure of cancer can be achieved. Another interesting topic is to incorporate exercise. Exercise is shown to solely suppress tumor growth through mobilization of natural killer cells [83]. The finding indicates that exercise may not just benefit the function and life quality of patients, but actually exerts some direct therapeutic efficacy [84].

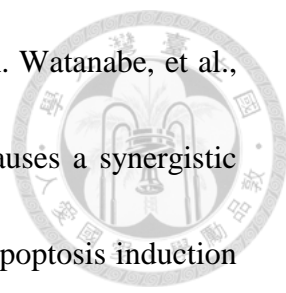
On the other hand, we will explore the mechanisms underlying the effects which pulsed-wave ultrasound directly acts on cancer cells, either by interacting with membranous structures or disrupting plasma membrane. We will also see if these mechanisms behave differently between malignant cells and normal cells. If so, these distinctions may provide the specificity required to design an anti-cancer therapy and therefore may lead to a novel therapeutic strategy. Then we will test different sets of ultrasound parameters (acoustic intensity, ultrasound frequency, pulse repetition frequency, etc.) to optimize the treatment efficacy. Furthermore, with knowledge about mechanisms behind bioeffects of pulsed-wave ultrasound, we may expand the applications of pulsed-wave ultrasound, such as immunomodulation and neuromodulation.

References



- [1] D. Hanahan, R.A. Weinberg, The hallmarks of cancer, *Cell* 100 (2000) 57–70.
- [2] D. Hanahan, R.A. Weinberg, Hallmarks of cancer: the next generation, *Cell* 144 (2011) 646–674.
- [3] K. Greish, Enhanced permeability and retention of macromolecular drugs in solid tumors: a royal gate for targeted anticancer nanomedicines, *J. Drug Target.* 15 (2007) 457–464.
- [4] K. Greish, Enhanced permeability and retention (EPR) effect for anticancer nanomedicine drug targeting, *Methods Mol. Biol.* 624 (2010) 25–37.
- [5] X. Wang X, Y. Wang, D.M. Shin, Advances of cancer therapy by nanotechnology, *Cancer Res. Treat.* 41 (2009) 1–11.
- [6] E. Piktel, K. Niemirowicz, M. Wątek, T. Wollny, P. Deptuła, R. Bucki, Recent insights in nanotechnology-based drugs and formulations designed for effective anti-cancer therapy, *J. Nanobiotechnology* 14 (2016) 39
- [7] H. Maeda, Y. Matsumura, Tumoritropic and lymphotropic principles of macromolecular drugs, *Crit. Rev. Ther. Drug Carrier Syst.* 6 (1989) 193–210.
- [8] Y. Matsumura, H. Maeda, A new concept for macromolecular therapeutics in cancer chemotherapy: mechanism of tumoritropic accumulation of proteins and the antitumor agent smancs, *Cancer Res.* 46 (1986) 6387–6392.

- 
- [9] G.L. Scherphof, J. Dijkstra, H.H. Spanjer, J.T. Derksen, F.H. Roerdink, Uptake and intracellular processing of targeted and nontargeted liposomes by rat Kupffer cells *in vivo* and *in vitro*, *Ann. N. Y. Acad. Sci.* 446 (1985) 368–384.
- [10] M.L. Immordino, F. Dosio, L. Cattel, Stealth liposomes: review of the basic science, rationale, and clinical applications, existing and potential, *Int. J. Nanomedicine* 1 (2006) 297–315.
- [11] M.L. Immordino, P. Brusa, S. Arpicco, B. Stella, F. Fosio, L. Cattel, Preparation, characterization, cytotoxicity and pharmacokinetics of liposomes containing docetaxel, *J. Control. Release* 91 (2003) 417–429.
- [12] S. Toraya-Brown, S. Fiering, Local tumour hyperthermia as immunotherapy for metastatic cancer, *Int. J. Hyperthermia* 30 (2014) 531–539.
- [13] G. Kong, R.D. Braun, M.W. Dewhirst, Hyperthermia Enables Tumor-specific Nanoparticle Delivery: Effect of Particle Size, *Cancer Res.* 60 (2000) 4440–4445.
- [14] H.D. Suit, M. Shwayder, Hyperthermia: potential as an anti-tumor agent, *Cancer* 34 (1974) 122–129.
- [15] G.M. Hahn, J. Braun, I. Har-Kedar, Thermochemotherapy: synergism between hyperthermia (42–43 degrees) and adriamycin (of bleomycin) in mammalian cell inactivation, *Proc. Natl. Acad. Sci. U.S.A.* 72 (1975) 937–940.

- 
- [16] T. Yoshida, T. Kondo, R. Ogawa, L.B. Feril Jr., Q.L. Zhao, A. Watanabe, et al., Combination of doxorubicin and low-intensity ultrasound causes a synergistic enhancement in cell killing and an additive enhancement in apoptosis induction in human lymphoma U937 cells, *Cancer Chemother. Pharmacol.* 61 (2008) 559–567.
- [17] A. Jernberg, M.R. Edgren, R. Lewensohn, H. Wiksell, A. Brahme, Cellular effects of high-intensity focused continuous wave ultrasound alone and in combination with X-rays, *Int. J. Radiat. Biol.* 77 (2001) 127–135.
- [18] F. Lejbkowicz, S. Salzberg, Distinct sensitivity of normal and malignant cells to ultrasound *in vitro*, *Environ. Health Perspect.* 105 (Suppl 6) (1997) 1575–1578.
- [19] M.A. Buldakov, M.A. Hassan, P. Jawaid, N.V. Cherdyntseva, T. Kondo, Cellular effects of low-intensity pulsed ultrasound and X-irradiation in combination in two human leukaemia cell lines, *Ultrason. Sonochem.* 23 (2015) 339–346.
- [20] P. Loverock, G. ter Haar, Synergism between hyperthermia, ultrasound and gamma irradiation, *Ultrasound Med. Biol.* 17 (1991) 607–612.
- [21] H. Ashush, L.A. Rozenszajn, M. Blass, M. Barda-Saad, D. Azimov, J. Radnay, et al., Apoptosis induction of human myeloid leukemic cells by ultrasound exposure, *Cancer Res.* 60 (2000) 1014–1020.
- [22] Y. Tabuchi, H. Ando, I. Takasaki, L.B. Feril Jr., Q.L. Zhao, R. Ogawa, et al.,

Identification of genes responsive to low intensity pulsed ultrasound in a human leukemia cell line Molt-4, *Cancer Lett.* 246 (2007) 149–156.



[23] L.B. Feril Jr., T. Kondo, Q.L. Zhao, R. Ogawa, Enhancement of hyperthermia-induced apoptosis by non-thermal effects of ultrasound, *Cancer Lett.* 178 (2002) 63–70.

[24] G.K. Ogilvie, H.A. Reynolds, B.C. Richardson, C.W. Badger, S.A. Goss, E.C. Burdette, Performance of a multi-sector ultrasound hyperthermia applicator and control system: *in vivo* studies, *Int. J. Hypertherm.* 6 (1990) 697–705.

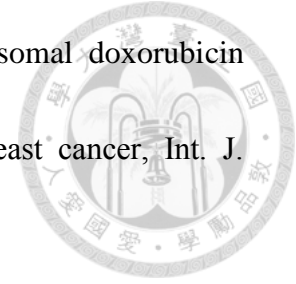
[25] F.L. Lizzi, M. Ostromogilsky, Analytical modelling of ultrasonically induced tissue heating, *Ultrasound Med. Biol.* 13 (1987) 607–618.

[26] C.A. Speed, Therapeutic ultrasound in soft tissue lesions, *Rheumatology (Oxford)* 40 (2001) 1331–1336.


[27] J.P. May, S.D. Li, Hyperthermia-induced drug targeting, *Exp. Opin. Drug Deliv.* 10 (2013) 511–527.

[28] Y. Liu, C.W. Cho, X. Yan, T.K. Henthorn, K.O. Lillehei, W.N. Cobb, et al., Ultrasound-Induced hyperthermia increases cellular uptake and cytotoxicity of P-glycoprotein substrates in multi-drug resistant cells, *Pharm. Res.* 18 (2001) 1255–1261.

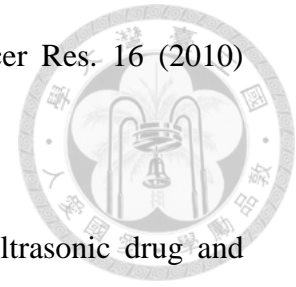
[29] S.K. Wu, C.F. Chiang, Y.H. Hsu, T.H. Lin, H.C. Liou, W.M. Fu, et al.,



- Short-time focused ultrasound hyperthermia enhances liposomal doxorubicin delivery and antitumor efficacy for brain metastasis of breast cancer, *Int. J. Nanomedicine* 9 (2014) 4485–4494.
- [30] V. Misik, P. Riesz, Free radical intermediates in sonodynamic therapy, *Ann. N. Y. Acad. Sci.* 899 (2000) 335–348
- [31] L.B. Feril Jr., T. Kondo, Z.G. Cui, Y. Tabuchi, Q.L. Zhao, H. Ando, et al., Apoptosis induced by the sonomechanical effects of low intensity pulsed ultrasound in a human leukemia cell line, *Cancer Lett.* 221 (2005) 145–152.
- [32] M.A. Buldakov, M.A. Hassan, Q.L. Zhao, L.B. Feril Jr., N. Kudo, T. Kondo, et al., Influence of changing pulse repetition frequency on chemical and biological effects induced by low-intensity ultrasound *in vitro*, *Ultrason. Sonochem.* 16 (2009) 392–397.
- [33] D.J. Kilonsky, Autophagy: from phenomenology to molecular understanding in less than a decade, *Nat. Rev. Mol. Cell Biol.* 8 (2007) 931-937.
- [34] R. Amaravadi, A.C. Kimmelman, E. White, Recent insights into the function of autophagy in cancer, *Genes Dev.* 30 (2006) 1913–1930.
- [35] E. White, Deconvoluting the context-dependent role for autophagy in cancer, *Nat. Rev. Cancer* 12 (2012) 401–410.
- [36] L. Galluzzi, F. Pietrocola, J.M. Bravo-San Pedro, R.K. Amaravadi, E.H.

- 
- Baehrecke, F. Cecconi, et al., Autophagy in malignant transformation and cancer progression, *EMBO J.* 34 (2015) 856–880.
- [37] J.M. Levy, A. Thorburn, Targeting autophagy during cancer therapy to improve clinical outcomes, *Pharmacol. Ther.* 131 (2011) 130–141.
- [38] J.M. Levy, C.G. Towers, A. Thorburn, Targeting autophagy in cancer, *Nat. Rev. Cancer* 17 (2017) 528–542.
- [39] A. Gupta, S. Roy, A.J. Lazar, W.L. Wang, J.C. McAuliffe, D. Reynoso, et al., Autophagy inhibition and anti-malarials promote cell death in gastrointestinal stromal tumor (GIST), *Proc. Natl. Acad. Sci. U.S.A.* 107 (2010) 14333–14338.
- [40] A. Balic, M.D. Sørensen, S.M. Trabulo, B. Sainz Jr., M. Cioffi, C.R. Vieira, et al., Chloroquine targets pancreatic cancer stem cells via inhibition of CXCR4 and hedgehog signaling, *Mol. Cancer Ther.* 13 (2014) 1758–1771.
- [41] H. Maes, A. Kuchnio, A. Peric, S. Moens, K. Nys, K. De Bock, et al., Tumor vessel normalization by chloroquine independent of autophagy, *Cancer Cell* 26 (2014) 190–206.
- [42] M. Thanou, W. Gedroyc, MRI-guided focused ultrasound as a new method of drug delivery, *J. Drug Deliv.* 2013 (2013) 616197.
- [43] P.R. Lockman, R.K. Mittapalli, K.S. Taskar, V. Rudraraju, B. Gril, K.A. Bohn, et al., Heterogeneous blood-tumor barrier permeability determines drug efficacy in

experimental brain metastases of breast cancer, *Clin. Cancer Res.* 16 (2010) 5664–5678.



[44] G.A. Husseini, W.G. Pitt, Micelles and nanoparticles for ultrasonic drug and gene delivery, *Adv. Drug Deliv. Rev.* 60 (2008) 1137–1152.

[45] S. Mitragotri, Healing sound: the use of ultrasound in drug delivery and other therapeutic applications, *Nat. Rev. Drug Discov.* 4 (2005) 255–260.

[46] W.G. Pitt, G.A. Husseini, B.J. Staples, Ultrasonic drug delivery—a general review, *Exp. Opin. Drug Deliv.* 1 (2004) 37–56.


[47] V. Frenkel, Ultrasound mediated delivery of drugs and genes to solid tumors, *Adv. Drug Deliv. Rev.* 60 (2008) 1193–1208.

[48] J.L. Nelson, B.L. Roeder, J.C. Carmen, F. Roloff, W.G. Pitt, Ultrasonically activated chemotherapeutic drug delivery in a rat model, *Cancer Res.* 62 (2002) 7280–7283.

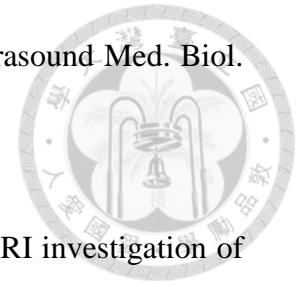
[49] C.R. Mayer, R. Bekeredjian, Ultrasonic gene and drug delivery to the cardiovascular system, *Adv. Drug Deliv. Rev.* 60 (2008) 1177–1192.

[50] O.J. Muller, H.A. Katus, R. Bekeredjian, Targeting the heart with gene therapy-optimized gene delivery methods, *Cardiovasc. Res.* 73 (2007) 453–462.

[51] K. Hynynen, Ultrasound for drug and gene delivery to the brain, *Adv. Drug Deliv. Rev.* 60 (2008) 1209–1217.

- 
- [52] H.R. Guzman, D.X. Nguyen, S. Khan, M.R. Prausnitz, Ultrasound-mediated disruption of cell membranes. II. Heterogeneous effects on cells, *J. Acoust. Soc. Am.* 110 (2001) 597–606.
- [53] S.B. Stringham, M.A. Viskovska, E.S. Richardson, S. Ohmine, G.A. Hussein, et al., Over-pressure suppresses ultrasonic-induced drug uptake, *Ultrasound Med. Biol.* 35 (2009) 409–415.
- [54] W. Tang, Q. Liu, X. Wang, P. Wang, B. Cao, N. Mi, et al., Involvement of caspase 8 in apoptosis induced by ultrasound-activated hematoporphyrin in sarcoma 180 cells *in vitro*, *J. Ultrasound Med.* 27 (2008) 645–656.
- [55] L.B. Feril Jr., T. Kondo, Biological effects of low intensity ultrasound: the mechanism involved, and its implications on therapy and on biosafety of ultrasound, *J Radiat Res* 45 (2004) 479–489.
- [56] M.A. Hassan, M.A. Buldakov, R. Ogawa, Q.L. Zhao, Y. Furusawa, et al., Modulation control over ultrasound-mediated gene delivery: evaluating the importance of standing waves, *J. Control. Release* 141 (2010) 70–76.
- [57] N. Wang, J.D. Tytell, D.E. Ingber, Mechanotransduction at a distance: mechanically coupling the extracellular matrix with the nucleus, *Nat. Rev. Mol. Cell Biol.* 10 (2009) 75–82.
- [58] W. Zhong, W.H. Sit, J.M. Wan, A.C. Yu, Sonoporation induces apoptosis and

cell cycle arrest in human promyelocytic leukemia cells, *Ultrasound Med. Biol.* 37 (2011) 2149–2159.



[59] N. McDannold, N. Vykhodtseva, F.A. Jolesz, K. Hynynen, MRI investigation of the threshold for thermally induced blood-brain barrier disruption and brain tissue damage in the rabbit brain, *Magn. Reson. Med.* 51 (2004) 913–923.

[60] A. Geser, G. Brubaker, C.C. Draper, Effect of a malaria suppression program on the incidence of African Burkitt's lymphoma, *Am. J. Epidemiol.* 129 (1989) 740–752.

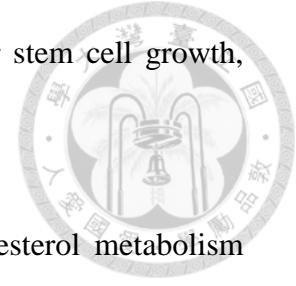
[61] S.K. Wu, C.F. Chiang, Y.H. Hsu, H.C. Liou, W.M. Fu, W.L. Lin, Pulsed-wave low-dose ultrasound hyperthermia selectively enhances nanodrug delivery and improves antitumor efficacy for brain metastasis of breast cancer, *Ultrason. Sonochem.* 36 (2017) 198–205.

[62] Y.W. Tsang, K.H. Chi, C.C. Huang, M.S. Chi, H.C. Chiang, K.L. Yang, et al., Modulated electro-hyperthermia-enhanced liposomal drug uptake by cancer cell, *Int. J. Nanomedicine* 14 (2019) 1269–1279.

[63] H.A. Hirsch, D. Iliopoulos, P.N. Tsiichlis, K. Struhl, Metformin selectively targets cancer stem cells, and acts together with chemotherapy to block tumor growth and prolong remission, *Cancer Res.* 69 (2009) 7507–7511.

[64] H.A. Hirsch, D. Iliopoulos, K. Struhl, Metformin inhibits the inflammatory

response associated with cellular transformation and cancer stem cell growth,
Proc. Natl. Acad. Sci. U.S.A. 110 (2013) 972–977.



[65] M.A. King, I.G. Ganley, V. Flemington, Inhibition of cholesterol metabolism underlies synergy between mTOR pathway inhibition and chloroquine in bladder cancer cells, *Oncogene* 35 (2016) 4518–4528.

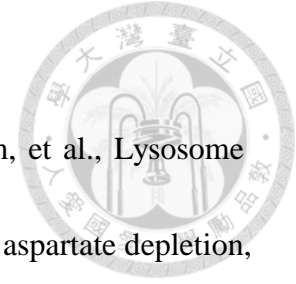
[66] D.S. Choi, E. Blanco, Y.S. Kim, A.A. Rodriguez, H. Zhao, T.H. Huang, et al., Chloroquine eliminates cancer stem cells through deregulation of Jak2 and DNMT1, *Stem Cells* 32 (2014) 2309–2323.

[67] M.F. Wei, M.W. Chen, K.C. Chen, P.J. Lou, S.Y. Lin, S.C. Hung, et al., Autophagy promotes resistance to photodynamic therapy-induced apoptosis selectively in colorectal cancer stem-like cells, *Autophagy* 10 (2014) 1179–1192.

[68] S.W. Lee, H.K. Kim, N.H. Lee, H.Y. Yi, H.S. Kim, S.H. Hong, et al., The synergistic effect of combination temozolomide and chloroquine treatment is dependent on autophagy formation and p53 status in glioma cells, *Cancer Lett.* 360 (2015) 195–204.

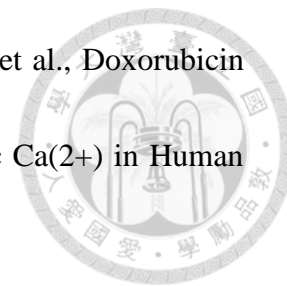
[69] P. Maycotte, C.M. Gearheart, R. Barnard, S. Aryal, J.M. Levy, S.P. Foslire, et al., STAT3-mediated autophagy dependence identifies subtypes of breast cancer where autophagy inhibition can be efficacious, *Cancer Res.* 74 (2014)

2579–2590.



- [70] I.A. Elliott, A.M. Dann, S. Xu, S.S. Kim, E.R. Abt, W. Kim, et al., Lysosome inhibition sensitizes pancreatic cancer to replication stress by aspartate depletion, *Proc. Natl. Acad. Sci. U.S.A.* 116 (2019) 6842–6847.
- [71] M.B. Schaaf, D. Houbaert, O. Meçe, S.K. To, M. Ganne, H. Maes, et al., Lysosomal pathways and autophagy distinctively control endothelial cell behavior to affect tumor vasculature, *Front. Oncol.* 20 (2019) 171.
- [72] W. Yang, G.H. Han, H.Y. Shin, E.J. Lee, H. Cho, D.B. Chay, et al., Combined treatment with modulated electro-hyperthermia and an autophagy inhibitor effectively inhibit ovarian and cervical cancer growth, *Int. J. Hyperthermia* 14 (2018) 1–12.
- [73] M.C. Ba, H. Long, S.Z. Cui, Y.F. Gong, Z.F. Yan, S. Wang, et al., Mild Hyperthermia enhances sensitivity of gastric cancer cells to chemotherapy through reactive oxygen species-induced autophagic death, *Tumor Biol.* 39 (2017) 1–9.
- [74] J.J. Bartlett, P.C. Trivedi, T. Pulinilkunnil, Autophagic dysregulation in doxorubicin cardiomyopathy, *J. Mol. Cell Cardiol.* 104 (2017) 1–8.
- [75] N. Koleini, E. Kardami, Autophagy and mitophagy in the context of doxorubicin-induced cardiotoxicity, *Oncotarget* 8 (2017) 46663–46680.

[76] J.H. Park, S.H. Choi, H. Kim, S.T. Ji, W.B. Jang, J.H. Kim, et al., Doxorubicin Regulates Autophagy Signals via Accumulation of Cytosolic Ca(2+) in Human Cardiac Progenitor Cells, *Int. J. Mol. Sci.* 17 (2016) E1680.



[77] D. Chen, J. Xie, R. Fiskesund, W. Dong, X. Liang, J. Lv, et al., Chloroquine modulates antitumor immune response by resetting tumor-associated macrophages toward M1 phenotype, *Nat. Commun.* 9 (2018) 873.

[78] J. Pelt, S. Busatto, M. Ferrari, E.A. Thompson, K. Mody, J. Wolfram, Chloroquine and nanoparticle drug delivery: A promising combination, *Pharmacol. Ther.* 191 (2018) 43–49.

[79] R. Sun, S. Shen, Y.J. Zhang, C.F. Xu, Z.T. Cao, L.P. Wen, et al., Nanoparticle-facilitated autophagy inhibition promotes the efficacy of chemotherapeutics against breast cancer stem cells, *Biomaterials* 103 (2016) 44–55.

[80] M. Shao, W. Zhu, X. Lv, Q. Yang, X. Liu, Y. Xie, et al., Encapsulation of chloroquine and doxorubicin by MPEG-PLA to enhance anticancer effects by lysosomes inhibition in ovarian cancer, *Int. J. Nanomedicine* 13 (2018) 8231–8245.

[81] J. Wolfram, S. Nizzero, H. Liu, F. Li, G. Zhang, Z. Li, et al., A chloroquine-induced macrophage-preconditioning strategy for improved

nanodelivery, *Sci. Rep.* 7 (2017) 13738.

[82] T. Lv, Z. Li, L. Xu, Y. Zhang, H. Chen, Y. Gao, Chloroquine in combination with aptamer-modified nanocomplexes for tumor vessel normalization and efficient erlotinib/Survivin shRNA co-delivery to overcome drug resistance in EGFR-mutated non-small cell lung cancer, *Acta Biomater.* 76 (2018) 257–274.

[83] L. Pedersen, M. Idorn, G.H. Olofsson, B. Lauenborg, I. Nookaew, R.H. Hansen, et al., Voluntary Running Suppresses Tumor Growth through Epinephrine- and IL-6-Dependent NK Cell Mobilization and Redistribution, *Cell Metab.* 23 (2016) 554–562.

[84] M. Idorn, P. thor Straten, Exercise and cancer: from "healthy" to "therapeutic"? *Cancer Immunol. Immunother.* 66 (2017) 667–671.

